Archive of Applied Mechanics (2023) 93:785–812
https://doi.org/10.1007/s00419-022-02299-8

ORIGINAL

T. S. Amer · S. A. Abdelhfeez · Rewan F. Elbaz

Modeling and analyzing the motion of a 2DOF dynamical tuned absorber system close to resonance

Received: 30 July 2022 / Accepted: 18 October 2022 / Published online: 31 October 2022

Abstract This work investigates the planar motion of a dynamical model with two degrees-of-freedom (DOF) consisting of a connected tuned absorber with a simple pendulum. It is taken into account that the pendulum's pivot moves in a Lissajous trajectory with stationary angular velocity in the presence of a harmonic excitation moment. In terms of the model's generalized coordinates, Lagrange's equations are used to derive the motion's controlling system. The approximate solutions of this system, up to a higher order of approximation, are achieved utilizing the approach of multiple scales (AMS). Resonance cases are all classified, in which two of them are examined simultaneously to gain the corresponding equations of modulation. The solutions at the steady-state are studied in terms of solvability conditions. According to the Routh-Hurwitz criteria, all potential fixed points at steady and unsteady states are determined and graphed. The dynamical behavior of the motion's time-histories and the curves of resonance are drawn. Regions of stability are examined by inspecting their graphs in order to assess the favorable impact of various parameters on the motion. The achieved outcomes are regarded as novel because the used methodology is applied to a specific dynamical system. The importance of this model under study can be seen from its numerous applications in disciplines like engineering and physics. Furthermore, pendulum vibration absorbers are commonly employed to reduce the vibrations in engineering constructions such as chimneys, bridges, television towers, high buildings, auto-balancing shafts, and antennas.

Keywords Vibrational motion · Nonlinear dynamics · Absorbers systems · Stability · Perturbation methods · Fixed points

1 Introduction

It is well known that vibrations and dynamic chaos are undesirable phenomena, especially in structures. They have the potential to disrupt, annoy, injure, or damage the various dynamical systems or structures. Therefore, effort, time, and money are expended to eliminate or reduce vibrations, disorder, and noise. Consequently, controlling on the vibrations is considered as a current problem. Many methods have been developed to absorb these vibrations to achieve the stabilization cases of different dynamic systems. In addition, there are an excessive number of developed smart materials for this reason.

T. S. Amer (✉)
Mathematics Department, Faculty of Science, Tanta University, Tanta 31527, Egypt
e-mail: tarek.saleh@science.tanta.edu.eg

S. A. Abdelhfeez · R. F. Elbaz
Department of Mathematics, Faculty of Science, Port Said University, Port Said, Egypt
e-mail: samy_abdelhafeez@sci.psu.edu.eg

R. F. Elbaz
e-mail: rewanelbaz@sci.psu.edu.eg

Mechanical structures must be developed to enable us for obtaining better performance under various types of loading, especially dynamic and temporal loads. One of the most common control methods is a vibration absorber. It is a supplementary system that is linked to a main one. As a result, the system gains a new degree of freedom. The absorber's parameters are selected in order to minimize or cancel the primary system's vibration. When the system is in main resonance, there is a good chance that it will be damaged; the absorber is often intended to control one mode or one frequency. In most circumstances when vibration must be decreased, a rectilinear motion is performed by the primary system. When a tuned absorber consists of a spring, a mass, and occasionally a damper, the motion can be rectilinear, but when dealing with a swinging pendulum, the rotating motion can be considered [1]. In [2], the authors investigated a dynamic absorber, in which it can be moved in a transverse direction or a longitudinal one, and is coupled to a simple pendulum that is externally triggered.

Many scientists have been interested in studying active vibration control [3–9]. In [3], the authors presented an approach for analyzing the structures using active and passive control systems, while a feedback of an optimal displacement control rule is constructed in [4] for a single DOF structure with an active tuned mass damper. In [5] and [6], the authors examined a basic pendulum connected with one tuned absorber in either the transverse or longitudinal directions. Negative velocity feedback or its square or cubic value is used to provide controllability to the system. Moreover, a feedback of reverse acceleration and angular displacement can be used besides their squares values or cubic ones to provide with an active control. Generalization of this work has been presented in [7] when a longitudinal absorber connected with the simple pendulum, in which the system's pivot point moves in a route of ellipse. Recently, the behavior of a dynamical system composed of a damped linear tuned-absorber in a transverse direction of a nonlinear damped-spring-pendulum whose hanging point rotates on an elliptic route is studied in [8]. Using the AMS, the approximate solutions for the controlling system are obtained up higher order of approximation. The conditions of Routh Hurwitz [10] have been used to investigate the stability and instability zones, and the results are compared with the steady-state solutions. A limited case from this work can be found in [9] for a fixed pivot point of an elastic pendulum attached with a transverse absorber.

Vibrational motion is used to treat severe damage that occurs in high-rise buildings, such as tall building which has a long period and low damping rate. This makes it more sensitive to long-range earthquakes and records near the fault, including long-period components due to resonance. Therefore, special attention should be paid to the seismic protection of tall buildings [11]. In [12, 13], an adaptive-passive variable pendulum and a tuned mass damper (TMD) were used to control wind-induced vibrations in a tall building, while a revolutionary tuned mass damper that can retune its frequency and damping ratio in real-time to protect a structure over its entire life cycle is investigated in [14]. Recently, a high-rise structure is fitted in [15] with a passive adaptive pendulum stream eddy TMD, in the presence of four different soil conditions. In [16], the authors simplified a supported steel footbridge to be used as the test model with a single DOF system. More applications can be found in [17, 18].

It must be noted that the motion of a damped linear or nonlinear spring pendulums in different paths has piqued the curiosity of many academics [19–32]. The analytic approximate solution of the nonlinear controlling equations of an elastic pendulum whose suspension point oscillates vertically in investigated in [19]. Whereas, a mathematical pendulum's planar rotational motion, where its fulcrum point oscillates vertically and horizontally, is examined in [20]. The stability and performance of the obtained solutions are established. On the other hand, the rotatory movements of a suspension point of a spring pendulum on an elliptic trajectory and on a closed Lissajous curve near resonance cases are investigated in [21, 22], respectively. Some prescribed motions as limited cases are presented. In [23], the authors examined the movement of a 3DOF dynamical system in a plane of a damped linear spring connected to a rigid body. The point of suspension is considered to be fixed. The generalizations of this problem are studied in [24] (for linear spring) and [25] (for nonlinear spring) when their pivot points rotate in elliptic trajectories. More descriptions of the rigid body pendulum can be found in [26] and [27]. The approximate solutions are obtained using the AMS, in which the corresponding equations of modulation are gained in light of the solvability requirements. The motion of a 2DOF auto-parametric dynamical model consisting of a coupled rolling cylinder and a damped spring is examined in [28]. The nonlinear stability of this system is investigated in view of the Routh-Hurwitz Criteria. The rotational motion of a charged gyro around a fixed point is investigated in [29] when some external moments and forces are applied. The approximate solutions are obtained using the approach of small parameter and represented graphically. The planar movement of a heavy solid attached to a string from one end and the other end moves in a specified trajectory is investigated analytically and numerically in [30] using the approach of large parameter and [31] applying the Runge–Kutta algorithms, respectively. On the other hand, the motion of a spring in a

plane is studied in [32] when its suspension point has a trajectory of a circle with sufficiently large radius. Computer codes are used to show the effect of the system's parameters on the examined motion. The nonlinear stability analysis for various motions of oscillating systems under harmonic external forces and torques is examined in [23–37].

In this study, the planar motion of a 2DOF dynamical model consisting of a coupled tuned longitudinal absorber with a simple pendulum is studied. This movement is devoted under the existence of an external harmonic excitation moment, in which the pendulum's pivot is constrained to move in a Lissajous trajectory with stationary angular velocity. Lagrange's equations are utilized to derive the governing EOM in light of the model's generalized coordinates. The AMS is used to estimate their solutions analytically till the third-order of approximation. Various classifications for resonance cases are presented, in which two of them are examined at the same time. As a result, the corresponding equations of modulation are obtained. The solvability criteria for the solutions at the steady-state are studied. The criteria of Routh-Hurwitz are used to find and graph all feasible fixed points at steady and unstable states. Modified phases and amplitudes, as well as the solutions' temporal histories, and resonance curves are graphed to investigate the dynamical behavior of the dynamical model at any instant. The impact of various parameters on the system's behavior is evaluated by checking the different stability regions. The significance of the investigated dynamical model can be observed in its several applications in practical life, especially in reducing vibrations that arise in various engineering structures.

The calculations were performed using the symbolic manipulation Wolfram Mathematica software (Mathematica_12.1.0_WIN_DLM: https://nsaneforums.com/topic/394731-wolfram-mathematica-v122-download-manager/). The majority of processes are performed automatically, owing to unique procedures developed by the authors.

2 Description of the problem

In this section, a full description of the examined model is presented, in which the EOM are derived and transformed to their dimensionless forms. Therefore, we consider the planar motion of a 2DOF dynamical model comprises of a simple pendulum of known mass M and with arm's length l besides its connection with a nonlinear absorber of mass m, which can only move in a longitudinal direction. It is considered that the pendulum's pivot point O follows a Lissajous curve, in an anticlockwise rotation, harmonically in two mutually perpendicular directions (see Fig. 1). As a result, the coordinates of this point are

$$x = R_x \cos(\Omega_x t)\,, \qquad y = R_y \sin(\Omega_y t), \tag{1}$$

where R_j $(j = x, y)$ and Ω_j are well-known parameters.

Let us consider O_1Y_1 and O_1X_1 to represent the vertical downward axis and the horizontal one, respectively, with the origin O_1. Furthermore, let φ be the rotation angle (the angle between the pendulum arm OA and the vertical at O), u is the absorber's longitudinal elongation from the equilibrium location, l_0 is the natural length of the absorber, c_1 and c_2 are the damping coefficients of rotation and absorber, $M(t) = f\cos(\Omega t)$ is the harmonic excitation rotation moment at O in which Ω is its frequency, and k_1 and k_2 are the spring's linear and nonlinear stiffness, respectively.

The model's kinetic and potential energies T and V have the forms

$$\begin{aligned}
T &= \frac{1}{2}(M+m)[\Omega_x^2 R_x^2 \sin^2(\Omega_x t) + \Omega_y^2 R_y^2 \cos^2(\Omega_y t)] + \frac{1}{2}\dot{\varphi}^2[M l^2 + m(l+l_0+u)^2] \\
&+ \frac{1}{2}m\dot{u}^2 + \dot{\varphi}\{(M l + m(l+l_0+u))[R_x\Omega_x \sin(\Omega_x t)\, \sin\varphi + R_y\Omega_y \cos(\Omega_x t)\cos\varphi]\} \\
&- m\dot{u}[R_x\Omega_x \sin(\Omega_x t)\cos\varphi - R_y\Omega_y \cos(\Omega_x t)\sin\varphi]. \\
V &= \frac{1}{2}k_1 u^2 + \frac{1}{4}k_2 u^4 - Mg[R_x\cos(\Omega_x t) + l\cos\varphi] - mg[R_x\cos(\Omega_x t) + (l+l_0+u)\cos\varphi].
\end{aligned} \tag{2}$$

Here, the letter g denotes the acceleration due to gravity and dots denote the derivatives regarding time t.

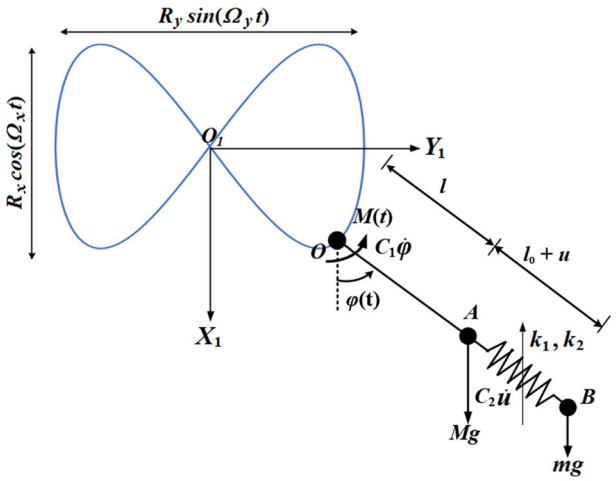

Fig. 1 Portrays the prescribed path of the dynamical model

Based on the latter equations, Lagrange's function $L = T - V$ can be immediately obtained, and then one can derive the regulating system of the EOM according to the model's generalized coordinates φ and u utilizing the following Lagrange's equations [38]

$$\begin{aligned} \frac{\mathrm{d}}{\mathrm{d}t}\left(\frac{\partial L}{\partial \dot{\varphi}}\right) - \frac{\partial L}{\partial \varphi} &= f\cos(\Omega t) - c_1\dot{\varphi}, \\ \frac{\mathrm{d}}{\mathrm{d}t}\left(\frac{\partial L}{\partial \dot{u}}\right) - \frac{\partial L}{\partial u} &= -c_2\dot{u}, \end{aligned} \tag{3}$$

To deal with the handled model, let us consider the following dimensionless forms

$$\begin{aligned} &l_1 = \frac{l_0}{l}, \quad m_1 = \frac{m}{m+M}, \quad r_x = \frac{R_x}{l}, \quad r_y = \frac{R_y}{l}, \quad \alpha = \frac{k_2 l^2}{m\omega_1^2}, \quad \omega_1^2 = \frac{g}{l}, \\ &\omega_2^2 = \frac{k_1}{m}, \quad \omega^2 = \frac{\omega_2^2}{\omega_1^2}, \quad u_1 = \frac{u}{l}, \quad C_1 = \frac{c_1}{\omega_1 l^2(m+M)}, \quad C_2 = \frac{c_2}{m\omega_1^2}, \\ &F = \frac{f}{\omega_1^2 l^2(m+M)}, \quad p_x = \frac{\Omega_x}{\omega_1}, \quad p_y = \frac{\Omega_y}{\omega_1}, \quad p = \frac{\Omega}{\omega_1}, \quad \tau = \omega_1 t. \end{aligned} \tag{4}$$

The substitution of (2) and (4) into (3), yields the next dimensionless forms of the controlling system

$$\begin{aligned} &[1 + m_1(l_1+u_1)(2+l_1+u_1)]\ddot{\varphi} + 2m_1(1+l_1+u_1)\dot{u}_1\,\dot{\varphi} + [1 + m_1(l_1+u_1)][p_x^2 r_x \cos p_x\tau \sin\varphi \\ &\quad - p_y^2 r_y \sin p_y\tau \cos\varphi] + \sin\varphi[1 + m_1(l_1+u_1)] + c_1\dot{\varphi} = F\cos p\tau, \end{aligned} \tag{5}$$

$$\ddot{u}_1 - (1+l_1+u_1)\dot{\varphi}^2 - p_x^2 r_x \cos p_x\tau\cos\varphi - p_y^2 r_y \sin p_y\tau \sin\varphi + \omega^2 u_1 + \alpha u_1^3 - \cos\varphi + c_2\dot{u}_1 = 0. \tag{6}$$

Here, the over dot represents the derivatives regarding τ. These equations represent a system of two nonlinear ordinary differential equations (ODE) of second order.

3 The perturbation methodology

The main purpose of this part is to acquire the approximate solutions of the governing system of EOM (5) and (6) utilizing the AMS up to the third-order of approximation in light of the exclusion of secular terms. To attain this objective, the trigonometric functions must be approximated using Taylor series up to the third-order in a way that is valid in a neighborhood region of static equilibrium. Therefore, introducing the following forms of $\sin\varphi$ and $\cos\varphi$ into Eqs. (5) and (6)

$$\sin\varphi \cong \left(\varphi - \frac{\varphi^3}{3!}\right), \quad \cos\varphi \cong \left(1 - \frac{\varphi^2}{2}\right), \tag{7}$$

to obtain the EOM in the forms

$$\begin{aligned}&\{1+m_1(l_1+u_1)[2+l_1+u_1]\}\ddot{\varphi}+2m_1(1+l_1+u_1)\dot{u}_1\dot{\varphi}\\&+[1+m_1(l_1+u_1)]\left[p_x^2r_x\left(\varphi-\frac{\varphi^3}{6}\right)\cos p_x\tau-p_y^2r_y\left(1-\frac{\varphi^2}{2}\right)\sin p_y\tau\right]\\&+\left(\varphi-\frac{\varphi^3}{6}\right)[1+m_1(l_1+u_1)]+c_1\dot{\varphi}=F\cos p\tau,\end{aligned}\tag{8}$$

$$\begin{aligned}&\ddot{u}_1-\left[p_x^2r_x\left(1-\frac{\varphi^2}{2}\right)\cos p_x\tau+p_y^2r_y\left(\varphi-\frac{\varphi^3}{6}\right)\sin p_y\tau\right]-(1+l_1+u_1)\dot{\varphi}^2+\omega^2u_1\\&+\alpha u_1^3-\left(1-\frac{\varphi^2}{2}\right)+c_2\dot{u}_1=0.\end{aligned}\tag{9}$$

It is worthy to note that, the functions u_1 and φ must be represented in terms of a small parameter $0<\varepsilon<<1$ in light of the new functions ϕ and Z according to

$$\varphi(\tau)=\varepsilon\,\phi(\tau;\varepsilon),\quad u_1(\tau)=\varepsilon\,Z(\tau;\varepsilon).\tag{10}$$

Based on AMS, the approximate solutions of these functions can be represented as a power series of ε as follows [39]

$$\begin{aligned}\phi&=\sum_{j=1}^{3}\varepsilon^{j-1}\phi_{j-1}(\tau_0,\,\tau_1,\,\tau_2)+O(\varepsilon^3),\\Z&=\sum_{j=1}^{3}\varepsilon^{j-1}Z_{j-1}(\tau_0,\,\tau_1,\,\tau_2)+O(\varepsilon^3),\end{aligned}\tag{11}$$

where $\tau_0=\tau,\ \tau_1=\varepsilon\tau$, and $\tau_2=\varepsilon^2\tau$ are distinct time scales, in which τ_0 and τ_1,τ_2 are known as the fast and slow time scales, respectively. Since we have a variety of scales, then the derivatives of τ can then be transformed to τ_n $(n=0,1,2)$ as follows

$$\begin{aligned}\frac{\mathrm{d}}{\mathrm{d}\tau}&=\frac{\partial}{\partial\tau_0}+\varepsilon\frac{\partial}{\partial\tau_1}+\varepsilon^2\frac{\partial}{\partial\tau_2},\\\frac{\mathrm{d}^2}{\mathrm{d}\tau^2}&=\frac{\partial^2}{\partial\tau_0^2}+2\varepsilon\frac{\partial^2}{\partial\tau_0\partial\tau_1}+\varepsilon^2\left(\frac{\partial^2}{\partial\tau_1^2}+2\frac{\partial^2}{\partial\tau_0\partial\tau_2}\right)+O(\varepsilon^3).\end{aligned}\tag{12}$$

The terms of $O(\varepsilon^3)$ are obviously ignored in (12) due to the smallness of them.

The damping parameters, amplitude of the force, and other parameters are assumed to be small according to the forms

$$\begin{aligned}&C_j=\varepsilon^2\tilde{C}_j\quad(j=1,2),\quad F=\varepsilon^3\tilde{F},\quad l_1=\varepsilon\tilde{l}_1,\\&m_1=\varepsilon\tilde{m}_1,\quad r_x=\varepsilon^2\tilde{r}_x,\quad r_y=\varepsilon^2\tilde{r}_y,\quad \alpha=\tilde{\alpha},\end{aligned}\tag{13}$$

where $\tilde{F},\tilde{l}_1,\tilde{C}_j,\tilde{m}_1,\tilde{\alpha},\tilde{r}_x$, and $\tilde{r}_y$ are parameters of order unity,

Substituting (10)–(13) into (8)–(9), and then equating the different coefficients of powers of ε in each side to construct the next groups of partial differential equations (PDE).

Equations of order (ε)

$$\frac{\partial^2\phi_0}{\partial\tau_0^2}+\phi_0=0,\tag{14}$$

$$\frac{\partial^2Z_0}{\partial\tau_0^2}+\omega^2Z_0=0.\tag{15}$$

Equations of order (ε^2)

$$\frac{\partial^2\phi_1}{\partial\tau_0^2}+\phi_1=-2\frac{\partial^2\phi_0}{\partial\tau_0\partial\tau_1}+p_y^2r_y\sin p_y\tau_0,\tag{16}$$

$$\frac{\partial^2 Z_1}{\partial \tau_0^2} + \omega^2 Z_1 = -2\frac{\partial^2 Z_0}{\partial \tau_0 \partial \tau_1} + p_x^2 r_x \cos p_x \tau_0 + \left(\frac{\partial \phi_0}{\partial \tau_0}\right)^2 - \frac{1}{2}\phi_0^2. \tag{17}$$

Equations of order (ε^3)

$$\frac{\partial^2 \phi_2}{\partial \tau_0^2} + \phi_2 = -2\frac{\partial^2 \phi_1}{\partial \tau_0 \partial \tau_1} - \frac{\partial^2 \phi_0}{\partial \tau_1^2} - 2\frac{\partial^2 \phi_0}{\partial \tau_0 \partial \tau_2} - 2\tilde{m}_1 \frac{\partial^2 \phi_0}{\partial \tau_0^2}(\tilde{l}_1 + Z_0) - 2\tilde{m}_1 \frac{\partial \phi_0}{\partial \tau_0}\frac{\partial Z_0}{\partial \tau_0}$$
$$- \phi_0 p_x^2 r_x \cos p_x \tau_0 + \frac{1}{6}\phi_0^3 - \tilde{m}_1 \phi_0 (\tilde{l}_1 + Z_0) - \tilde{C}_1 \frac{\partial \phi_0}{\partial \tau_0} + \tilde{F} \cos p\tau_0, \tag{18}$$

$$\frac{\partial^2 Z_2}{\partial \tau_0^2} + \omega^2 Z_2 = -2\frac{\partial^2 Z_1}{\partial \tau_0 \partial \tau_1} - \frac{\partial^2 Z_0}{\partial \tau_1^2} - 2\frac{\partial^2 Z_0}{\partial \tau_0 \partial \tau_2} + \phi_0 p_y^2 r_y \sin p_y \tau_0 + 2\frac{\partial \phi_0}{\partial \tau_0}\frac{\partial \phi_1}{\partial \tau_0}$$
$$- \tilde{\alpha} Z_0^3 + [\tilde{l}_1 + Z_0]\left(\frac{\partial \phi_0}{\partial \tau_0}\right)^2 + 2\frac{\partial \phi_0}{\partial \tau_0}\frac{\partial \phi_0}{\partial \tau_1} - \phi_0 \phi_1 - \tilde{C}_2 \frac{\partial Z_0}{\partial \tau_0}. \tag{19}$$

Our aim now is to solve the previous PDE (14)–(19), in which it can be solved successively. To accomplish this target, we start with the general solutions of the first group of Eqs. (14) and (15), which can be formulated as follows

$$\phi_0 = A_1 e^{i\tau_0} + \overline{A}_1 e^{-i\tau_0}, \tag{20}$$

$$Z_0 = A_2\, e^{i\omega\tau_0} + \overline{A}_2\, e^{-i\omega\tau_0}. \tag{21}$$

Here A_j $(j = 1, 2)$ and $\overline{A}_j$ are known as complex functions and their conjugates, in which they depend on τ_j.

Inserting these solutions into the second group of PDE (16)-(17) and then deleting terms that generate secular ones to find their removal criteria as below

$$\frac{\partial A_1}{\partial \tau_1} = 0, \qquad \frac{\partial A_2}{\partial \tau_1} = 0. \tag{22}$$

As a result of these criteria, we may write the solutions of the second group in the following forms

$$\phi_1 = -\frac{i\, p_y^2 \tilde{r}_y e^{ip_y\tau_0}}{2(1 - p_y^2)} + CC, \tag{23}$$

$$Z_1 = \frac{p_x^2 \tilde{r}_x e^{ip_x\tau_0}}{2(\omega^2 - p_x^2)} - \frac{3A_1^2 e^{2i\tau_0}}{2(\omega^2 - 4)} + \frac{A_1 \overline{A}_1}{\omega^2} + CC, \tag{24}$$

where CC denotes the conjugates of the foregoing terms.

To obtain the criteria of solvability for the approximation of third-order, substitute (20), (21), (23), and (24) into the last set of PDE (18) and (19), and then remove terms that yield the secular ones. Therefore, we can write

$$\tilde{m}_1 \tilde{l}_1 A_1 - 2i\frac{\partial A_1}{\partial \tau_2} + \frac{1}{2}A_1^2 \overline{A}_1 - i\tilde{C}_1 A_1 = 0, \tag{25}$$

$$2A_2 A_1 \overline{A}_1 - 2i\omega\frac{\partial \overline{A}_2}{\partial \tau_2} - 3\tilde{\alpha} A_2^2 \overline{A}_2 - i\omega \tilde{C}_2 A_2 = 0. \tag{26}$$

In light of these criteria, the third-order approximations can be given in the forms

$$\phi_2 = \frac{\tilde{m}_1(1 + 2\omega)}{[1 - (1 + \omega)^2]} A_1 A_2 e^{i(1+\omega)\tau_0} + \frac{\tilde{m}_1(1 - 2\omega)}{[1 - (1 - \omega)^2]} A_1 \overline{A}_2 e^{i(1-\omega)\tau_0} - \frac{p_x^2 \tilde{r}_x}{2[1 - (1 + p_x)^2]} A_1 e^{i(1+p_x)\tau_0}$$
$$- \frac{p_x^2 \tilde{r}_x}{2[1 - (1 - p_x)^2]} A_1 e^{i(1-p_x)\tau_0} - \frac{1}{48}A_1^3 e^{3i\tau_0} + \frac{\tilde{F} e^{ip\tau_0}}{2(1 - p^2)} + CC, \tag{27}$$

$$Z_2 = \frac{i\, A_1 p_y^2 e^{i(1+p_y)\tau_0}}{2[\omega^2 - (1 + p_y)^2]}\left[\frac{1 + 2p_y}{(1 - p_y^2)} - 1\right] + \frac{i\, A_1 e^{i(1-p_y)\tau_0}}{2[\omega^2 - (1 - p_y)^2]} + \frac{1}{8\omega^2}\tilde{\alpha} A_2^3 e^{3i\omega\tau_0}$$
$$- \frac{\tilde{l}_1 A_1^2 e^{2i\tau_0}}{(\omega^2 - 4)} + \frac{2}{\omega^2}\tilde{l}_1 A_1 \overline{A}_1 - \frac{A_1^2 A_2 e^{i(2+\omega)\tau_0}}{[\omega^2 - (2 + \omega)^2]} - \frac{A_1^2 \overline{A}_2 e^{i(2-\omega)\tau_0}}{[\omega^2 - (2 - \omega)^2]} + CC. \tag{28}$$

The functions A_j $(j = 1, 2)$ can be estimated using the removal criteria (22), (25), and (16) for secular terms. Therefore, the approximate solutions φ and u_1 can be easily obtained using the above derived solutions of first to third orders and the postulates (10).

4 Resonance categorizations and modulating equations

The categorizations of resonance cases that may emerge in the acquired solutions, as well as the evaluation of one of these cases, are both significant aspects of this section. We infer that these solutions are collapsed when any of their denominators equal zero [40]. As a result, the following cases can be recognized.

(i) The primary external resonance case can be discovered at $p \approx 1$,

(ii) The internal resonance case has been satisfied at $\omega = 0$, $\omega = \pm 2$, $\omega = \pm p_x$,$\omega = 1 \pm p_y$, $p_y = \pm 1$, $p_x = 0$, $p_x = \pm 2$.

It is important to keep in mind that if any one of the previous resonance instances is fulfilled, the examined system's behavior will become convoluted. Consequently, we ought to modify the used approach. To deal with this circumstance, we will look at one of primary external resonance and one of internal resonance that operate together, i.e., $p \approx 1$ and $\omega \approx 2$. These correlations show how closely p and ω to 1 and 2, respectively.

It is necessary to employ the dimensionless parameters known as detuning σ_j $(j = 1, 2)$, which measure the displacement from the oscillations to the tight resonance [39]. Then we can start writing

$$p = 1 + \sigma_1, \qquad 2 = 2\omega + \sigma_2. \tag{29}$$

Therefore, we can write them in terms of ε as follows

$$\sigma_j = \varepsilon \tilde{\sigma}_j \quad (j = 1,\ 2\,). \tag{30}$$

The criteria of solvability can be gained through the substitution of (29) and (30) into the second and third groups of PDE (16)-(19). Elimination of terms that yield the secular terms gives the next conditions.

Solvability criteria of the second group

$$\frac{\partial A_1}{\partial \tau} = 0, \quad \frac{\partial A_2}{\partial \tau} = 0. \tag{30}$$

Solvability criteria of the third group

$$\begin{aligned} &\tilde{m}_1 \tilde{l}_1 A_1 - 2i \frac{\partial A_1}{\partial \tau_2} + \frac{1}{2} A_1^2 \overline{A}_1 - i \tilde{C}_1 A_1 + \tilde{F} e^{i\tilde{\sigma}_1 \tau_1} = 0, \\ &2A_2 A_1 \overline{A}_1 - 2i\omega \frac{\partial A_2}{\partial \tau_2} - 3\tilde{\alpha} A_2^2 \overline{A}_2 - i\omega \tilde{C}_2 A_2 - A_1^2 \overline{A}_2 e^{i\tilde{\sigma}_2 \tau_1} = 0. \end{aligned} \tag{31}$$

This implies that the solvability criteria consist of four nonlinear PDE in which A_j $(j = 1,\ 2\,)$ depend only on τ_2, which motivates us to depict them in the following polar form

$$A_j(\tau_2) = \frac{\tilde{h}_j(\tau_2)}{2} e^{i\psi_j(\tau_2)}, \qquad h_j = \varepsilon \tilde{h}_j \quad (j = 1,\ 2), \tag{32}$$

where $\tilde{h}_j$ and ψ_j are real functions of the amplitudes and phases of the solutions φ and u_1.

The below indicated modified phases can be used to adapt the preceding solvability criteria from PDE to ordinary differential equations (ODE).

$$\begin{aligned} \theta_1(\tau_2) &= \tau_2 \tilde{\sigma}_1 - \psi_1(\tau_2), \\ \theta_2(\tau_2) &= \tau_2 \tilde{\sigma}_2 + 2[\psi_1(\tau_2) - \psi_2(\tau_2)]. \end{aligned} \tag{33}$$

Substituting (32) and (33) into (31), and then splitting the imaginary and real components to obtain the below four first-order modulation equations for the resonance cases under consideration

$$\begin{aligned} h_1 \frac{\mathrm{d}\theta_1}{\mathrm{d}\tau} &= \sigma_1 h_1 + \frac{1}{2} m_1 l_1 h_1 + \frac{1}{16} h_1^3 + \frac{F}{2} \cos\theta_1, \\ \frac{\mathrm{d}h_1}{\mathrm{d}\tau} &= -\frac{1}{2} C_1 h_1 + \frac{F}{2} \sin\theta_1, \\ \frac{\mathrm{d}\theta_2}{\mathrm{d}\tau} &= \sigma_2 + 2\sigma_1 - 2\frac{\mathrm{d}\theta_1}{\mathrm{d}\tau} - \frac{3}{4\omega} \alpha h_2^2 + \frac{h_1^2}{2\omega} \left(1 - \frac{1}{2} \cos\theta_2\right), \\ \frac{\mathrm{d}h_2}{\mathrm{d}\tau} &= -\frac{1}{2} C_2 h_2 - \frac{h_1^2 h_2}{8\omega} \sin\theta_2. \end{aligned} \tag{34}$$

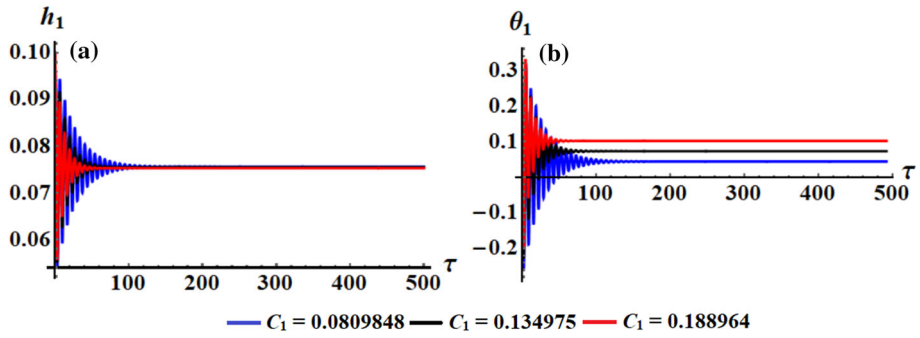

Fig. 2 Describes the influence of various values of C_1: **a** on the amplitude $h_1(\tau)$, **b** on the phase $\theta_1(\tau)$

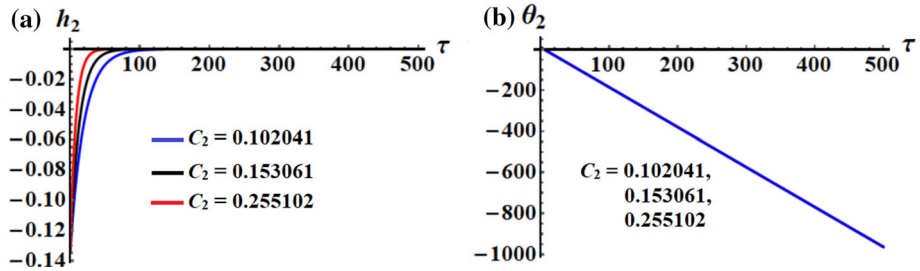

Fig. 3 Explores the impact of different values of C_2: **a** on the amplitude $h_2(\tau)$, **b** on the phase $\theta_2(\tau)$

The variation of the solutions h_j $(j = 1, 2)$ and θ_j of system (34) with time is drawn in Figs. 2 and 3, while the diagrams of the planes $\theta_j h_j$ are represented in Figs. 4 and 5 taking the following data into account

$$\begin{aligned} &\sigma_1 = -1.07114, \quad \sigma_2 = 0.192984, \quad l = 0.9, \quad l_0 = 0.6, \quad M = 12, \\ &m = 9\,, \quad R_x = 0.9\,, R_y = 1.2\,, \quad k_1 = 80, \quad k_2 = 11\,, \quad g = 9.8, \\ &\alpha = 0.0909184\,, \quad f = 26, \quad \Omega_x = 0.002, \quad \Omega_y = 0.003, \quad p = -0.07114\,. \end{aligned} \tag{35}$$

The time histories of h_1, θ_1 and h_2, θ_2 are calculated when $C_1(= 0.0809848, 0.134975, 0.188964)$ and $C_2(= 0.102041, 0.153061, 0.255102)$, respectively. The planes $\theta_1 h_1$ and $\theta_2 h_2$ are graphed in accordance with the same values of C_1 and C_2. The included curves in portions (a) and (b) of Fig. 2 oscillate rapidly around a fanciful horizontal symmetry axis at the first stage of the considered time interval and have a decay mode. Therefore, they have steady behavior till the end of the time interval. It is noticed that with the increasing of the values of damping coefficient C_1, the solutions h_1 and θ_1 reach faster to their steady case than the other little values. It is found that h_1 and θ_1 have not any variation with the various values of C_2. The reason is due to that their equations do not depend on C_2.

On the other hand, the represented curves of $h_2(\tau)$ and $\theta_2(\tau)$ are plotted in portions (a) and (b) of Fig. 3, which they are constitute with the solutions of the system of Eq. (34), in which they do not depend on C_1. Therefore, we cannot expect any variation with C_1. The corresponding phase plane curves of Figs. 2 and 3 are plotted in Fig. 4 with spiral curves and Fig. 5 with convex curves, respectively.

The time histories of the acquired approximate solutions (AS) $\varphi(\tau)$ and $u_1(\tau)$ are drawn in portions (a) and (b) of Fig. 6 when C_1 and C_2 have different values. An assessment of the included curves in these portions reveals that periodic waves and decay ones are produced for the solutions φ and u_1, respectively. Figure 7 depicts a comparison between the AS and numerical solutions (NS) of the governing system of motion, demonstrating their remarkable consistency. This indicates that the AS is precise with the used perturbation approach.

One of the important aspects of this research is to study the effect of various values of F, p_x, and p_y on the behavior of the amplitudes h_j $(j = 1, 2)$, phases θ_j, and the approximate solutions φ and u_1. Therefore, Figs. 8, 9, 10, 11 and12) are graphed according to the data (35) and with the variation of $F(= 0.10798, 0.140374, 0.188964)$, $p_x(= 0.00060609, 0.0303046, 0.0757614)$, and $p_y(= 0.0009091, 0.0242437, 0.0606092)$.

The indicated curves of portions of Figs. 8 and 9 show the variation of the time histories of h_1, θ_1 and h_2, θ_2 at the considered values of F, p_x, and p_y. It is clear that the change of the values of F has a good influence on

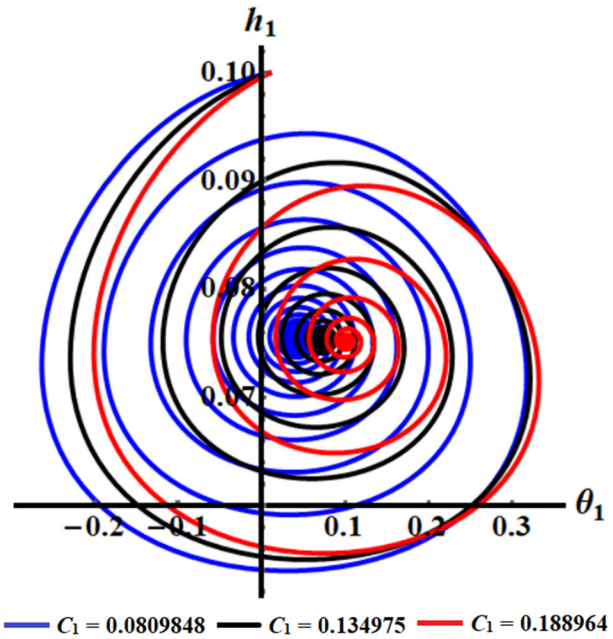

Fig. 4 Describes the plane curves $\theta_1 h_1$ for the values of C_1 as in Fig. 2

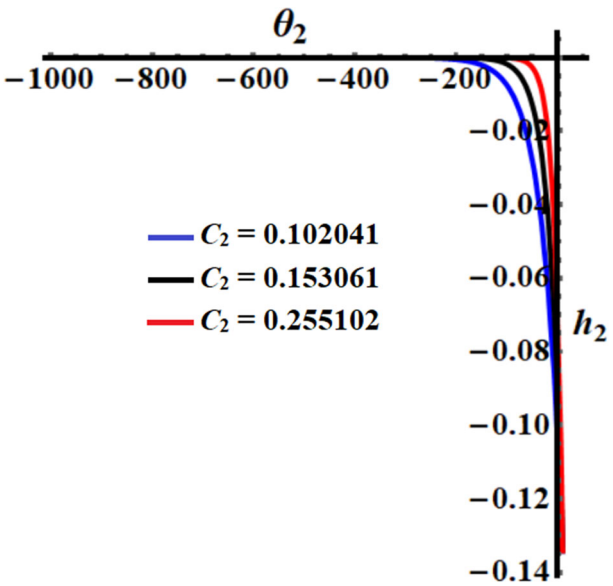

Fig. 5 Represents the plane curves $\theta_2 h_2$ for the values of C_2 as in Fig. 3

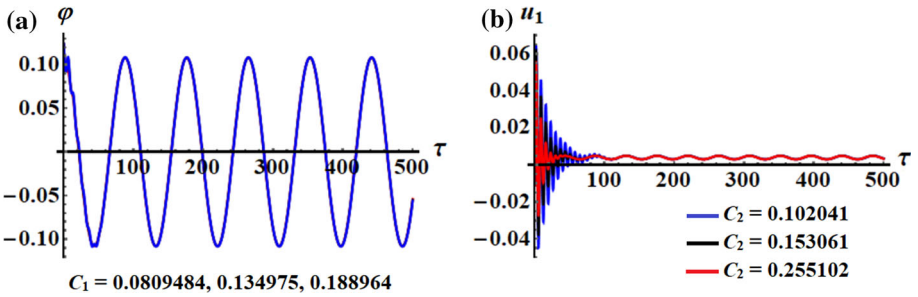

Fig. 6 Depicts the variation with τ for the functions: **a** φ at different values of C_1, **b** u_1 at different values of C_2

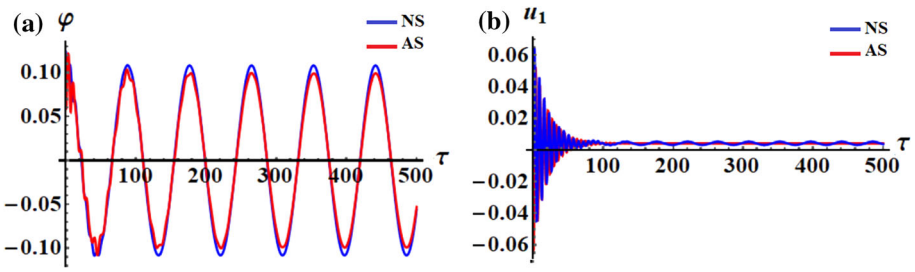

Fig. 7 Explores the differences between the NS and the AS for: **a** φ at $C_1 = 0.0809848$, **b** u_1 at $C_2 = 0.102041$

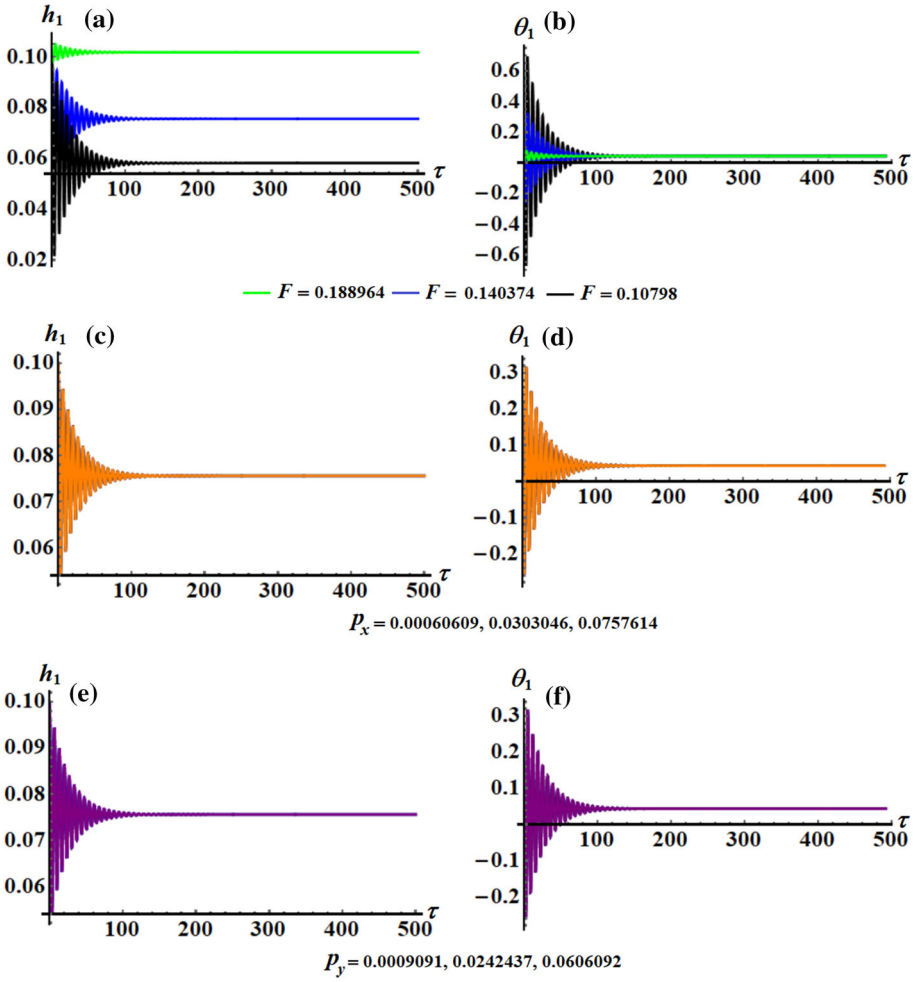

Fig. 8 Parts **a**, **b** reveal the influence of F, parts **c**, **d** describe the impact of p_x, and parts **e**, **f** show the change of p_y, on the time histories of h_1 and θ_1

the behavior of h_1 and θ_1 as seen in portions (a) and (b) of Fig. 8, while the influence of different values of p_x and p_y has a little effect, to some extent, on the time histories of h_1 and θ_1 as drawn in portions (c), (d), (e), and (f) of Fig. 8. The reason goes back to the formulation of Eq. (34). As plotted in Fig. 9, one can observe that there are no variations of the temporal histories of h_1 and θ_1 when F, p_x, and p_y take their mentioned values. The phase plane diagrams of these amplitudes h_j and phases θ_j are drawn in the planes $\theta_j h_j$, see portions (a), (b), and (c) of Figs. 10 and 11.

Curves of portions (a), (c), (e) and (b), (d), (f) show the behavior of the attained solutions $\varphi(\tau)$ and $u_1(\tau)$ when F, p_x, and p_y have the same considered values in drawing Figs. 8, 9, 10 and 11. As predicted from the equations of system (34) that φ and u_1 have an excellent influences with the values of F as seen in parts

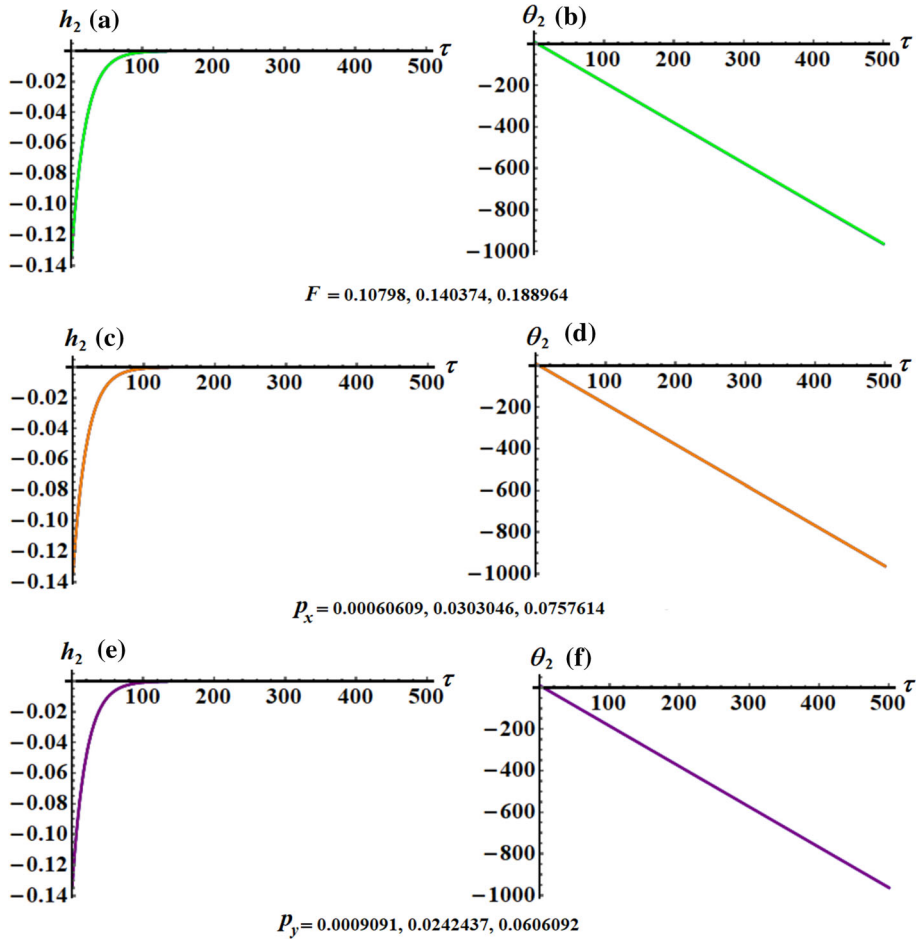

Fig. 9 Portions **a**, **b** reveal the influence of F, portions **c**, **d** describe the impact of p_x, and portions **e**, **f** show the change of p_y, on the time histories of h_2 and θ_2

(a), and (b) of Fig. 12. However, the behavior of φ has the form of standing periodic waves with some nodes, in which their amplitudes decrease with the increase in the values of F, as graphed in Fig. 12a. On the other hand, the variation of u_1 has a decaying pattern till the end of the investigated time interval. Therefore, these solutions have stable behaviors. As drawn in parts (c), (e) and (d), (f), one can conclude that the variations of φ and u_1 become stationary (to some extent) and slightly with the variation of the values of p_x and p_y, respectively.

5 Steady-state solutions

The main goal of this part is to explore the vibrations of the investigated system in the case of steady-state, in which it will appear when the transitory processes fade away. As a result, the left-hand sides of Eq. (34) will be regarded as zero, i.e., $dh_j/d\tau = d\theta_j/d\tau = 0$ $(j = 1, 2)$ [23, 27]. Then an algebraic system of four equations for the adjusted phases θ_j and the amplitudes h_j can be produced in the following form

$$\begin{aligned}
&\sigma_1 h_1 + m_1 l_1 h_1 + \frac{1}{16} h_1^3 + \frac{F}{2}\cos\theta_1 = 0,\\
&F\sin\theta_1 - C_1 h_1 = 0,\\
&\sigma_2 + 2\sigma_1 - \frac{3}{4\omega}\alpha h_2^2 + \frac{h_1^2}{4\omega}(2 - \cos\theta_2) = 0,\\
&C_2 h_2 + \frac{h_1^2 h_2}{4\omega}\sin\theta_2 = 0.
\end{aligned} \tag{36}$$

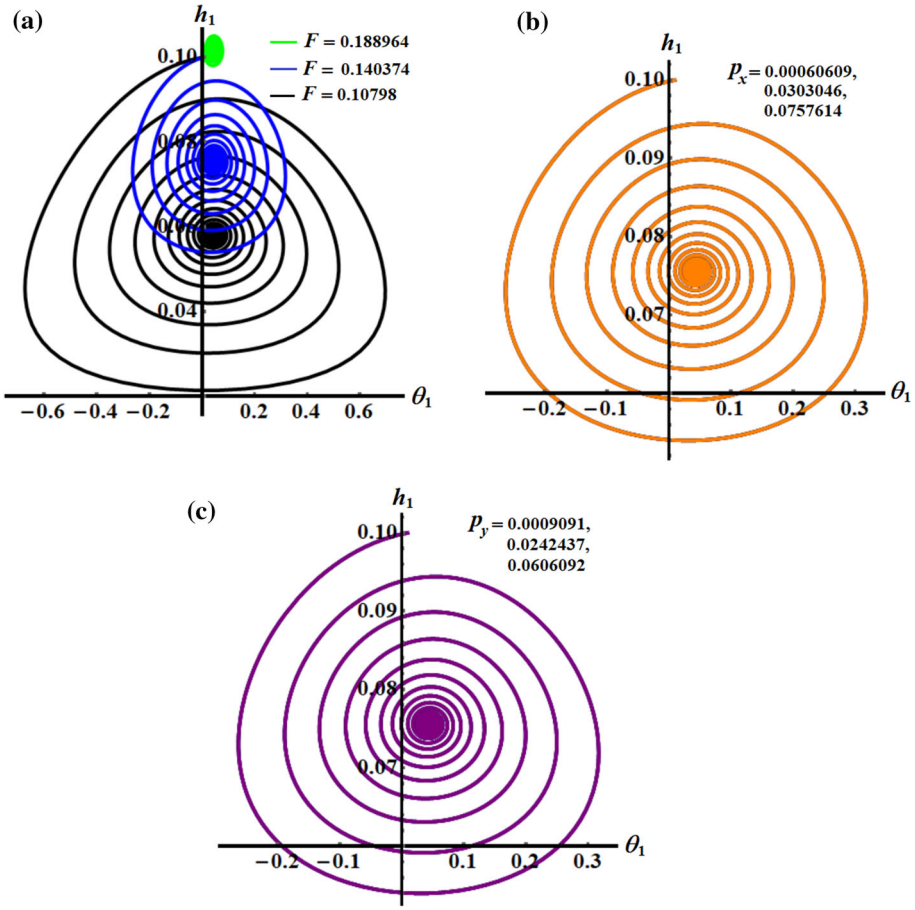

Fig. 10 Represents the curves in the planes $\theta_1 h_1$: **a** when F has different values, **b** at different values of p_x, **c** when p_y changes

A closer look at the aforementioned system (36), we can find the elimination of its adjusted phases θ_j yields the following functions of frequency response

$$F^2 = \left(\sigma_1 h_1 + m_1 l_1 h_1 + \frac{1}{16} h_1^3\right)^2 + C_1^2 h_1^2,$$
$$h_1^4 = 16\omega^2 \left[\left(\sigma_2 + 2\sigma_1 - \frac{3}{4\omega}\alpha h_2^2 + \frac{h_1^2}{2\omega}\right)^2 + C_2^2\right]. \tag{37}$$

These equations are clearly implicit formulations of nonlinear algebraic equations between h_j and σ_j. It is well recognized that one of the main stages in the steady-state vibrations is to look into the stability analysis of fixed points. Consequently, the system's behavior in an area near the fixed points is investigated. To achieve this goal, inserting the next substitutions in (34) [40]

$$h_1 = h_{10} + h_{11}, \qquad \theta_1 = \theta_{10} + \theta_{11},$$
$$h_2 = h_{20} + h_{21}, \qquad \theta_2 = \theta_{20} + \theta_{21}. \tag{38}$$

Here h_{j0} and θ_{j0} symbolize the solutions at the steady-state case of (34), while h_{j1} and θ_{j1} denote the perturbation that is very minor in relation to h_{j0} and θ_{j0}. Making use of (34) and (38) to obtain

$$h_{10}\frac{\mathrm{d}\theta_{11}}{\mathrm{d}\tau} = \sigma_1 h_{11} + \frac{1}{2}(m_1 l_1 h_{11} - F\theta_{11}\sin\theta_{10}) + \frac{3}{16}h_{10}^2 h_{11},$$
$$\frac{\mathrm{d}h_{11}}{\mathrm{d}\tau} = -\frac{1}{2}(C_1 h_{11} + F\theta_{11}\cos\theta_{10}),$$

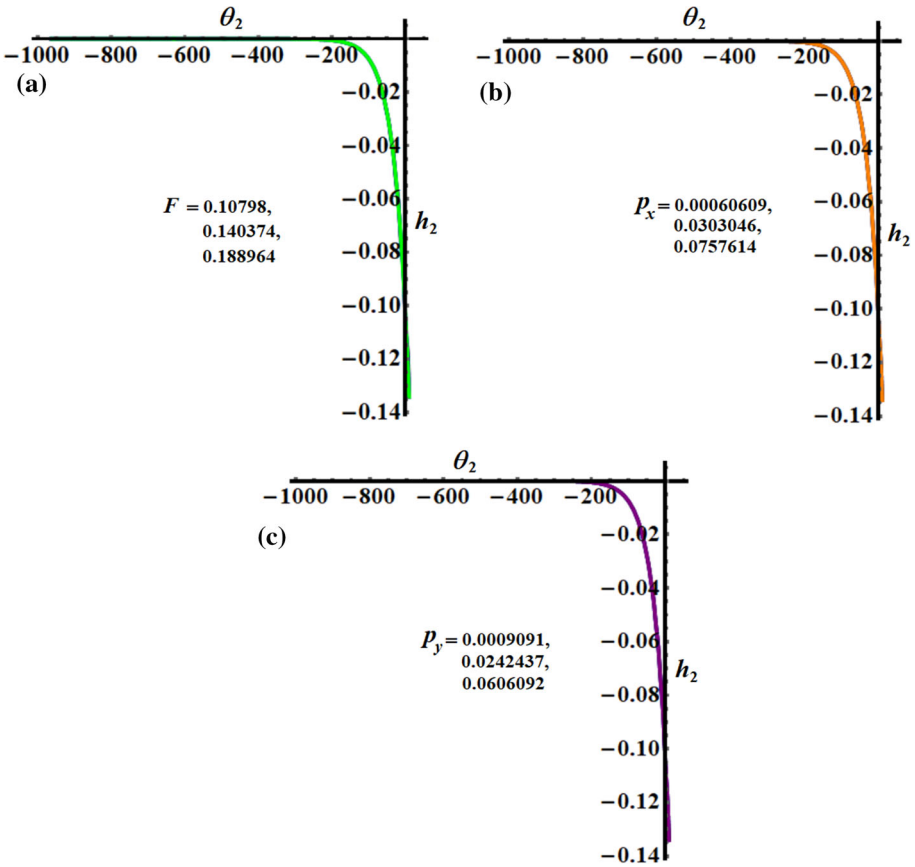

Fig. 11 Presents the curves in the planes $\theta_2 h_2$: **a** when F has different values, **b** at different values of p_x, **c** when p_y changes

$$h_{20}\frac{\mathrm{d}\theta_{21}}{\mathrm{d}\tau} = h_{21}(\sigma_2 + 2\sigma_1) - 2h_{20}\frac{\mathrm{d}\theta_1}{\mathrm{d}\tau} + \frac{1}{4\omega}(2h_{10}^2 h_{21} - 9\alpha h_{20}^2 h_{21} + 4h_{10}h_{20}h_{11} + h_{10}^2 h_{20}\theta_{21}\sin\theta_{20}),$$
$$\frac{\mathrm{d}h_{21}}{\mathrm{d}\tau} = -\frac{1}{2}C_2 h_{21} - \frac{h_{10}^2 h_{20}}{8\omega}\theta_{21}\cos\theta_{20}. \tag{39}$$

Taking into account that the functions $\theta_{j1}\,(j = 1, 2)$ and h_{j1} are unknown perturbed functions for the system of Eqs. (39). Then, their solutions can be represented as $k_s e^{\lambda T}$ $(s = 1, 2, 3, 4)$, where λ and k_s are the eigenvalues and constants of these functions, respectively. When the steady-state solutions are asymptotically stable, then the real potions' roots of the below characteristic equation of system (39) should be negative [10, 41]

$$\lambda^4 + \Gamma_1\lambda^3 + \Gamma_2\lambda^2 + \Gamma_3\lambda + \Gamma_4 = 0, \tag{40}$$

where Γ_s $(s = 1, 2, 3, 4)$ have the forms

$$\Gamma_1 = \frac{1}{4}\left[2C_1 + 2C_2 - \frac{2F\,\sin\theta_{10}}{h_{10}} - \frac{h_{10}^2\sin\theta_{20}}{\omega}\right],$$
$$\Gamma_2 = \frac{1}{32h_{10}\omega^2}[8C_1C_2\omega^2 h_{10} - F(3h_{10}^2 + 16\sigma_1)\omega^2\cos\theta_{10} + [2h_{10}^2 - 9h_{20}^2\alpha + 4(2\sigma_1 + \sigma_2)\omega]\cos\theta_{20}h_{10}^3 + 8(C_1 + C_2)F\omega^2\sin\theta_{10} - 4(C_1 + C_2)\omega \times \sin\theta_{20}h_{10}^3 - 4F\omega\,\sin\theta_{10}\,\sin\theta_{20}h_{10}^2 - 8F\omega^2 l_1 m_1\cos\theta_{10}],$$
$$\Gamma_3 = \frac{1}{128h_{10}\omega^2}\{F(3h_{10}^2 + 16\sigma_1)(h_{10}^2\sin\theta_{20} - 2C_2\omega)\omega\cos\theta_{10} + 2\{h_{10}^2[2h_{10}^2$$

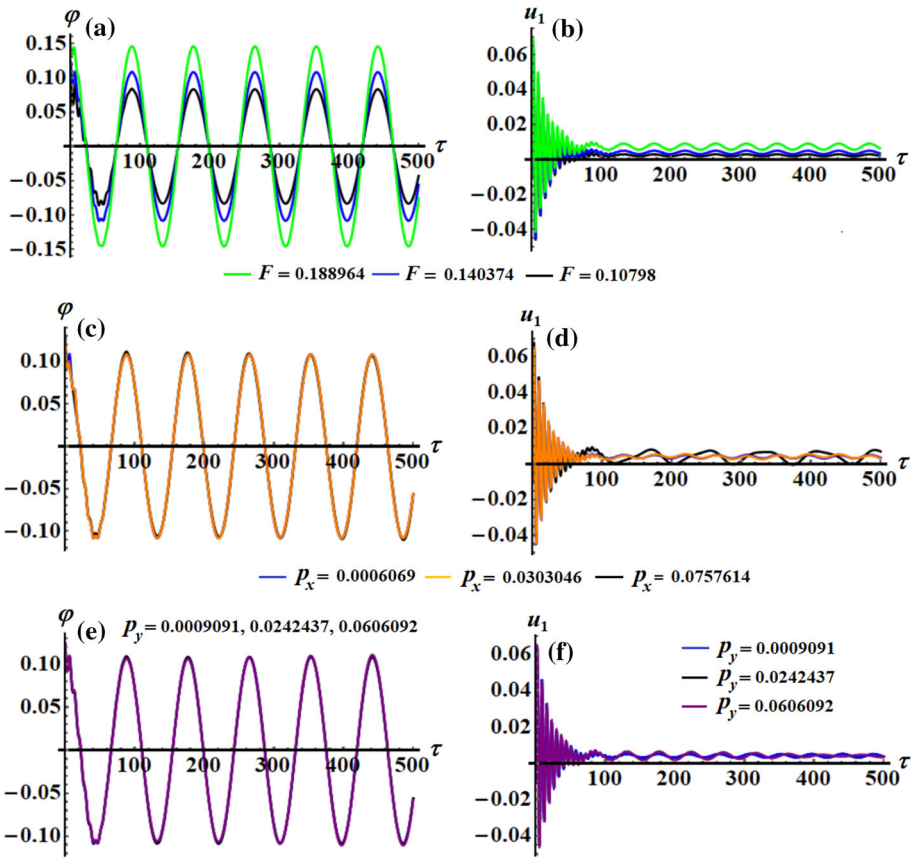

Fig. 12 Parts **a**, **b** reveal the influence of F, parts **c**, **d** describe the impact of p_x, and parts **e**, **f** show the change of p_y, on the solutions $\varphi(\tau)$ and $u_1(\tau)$

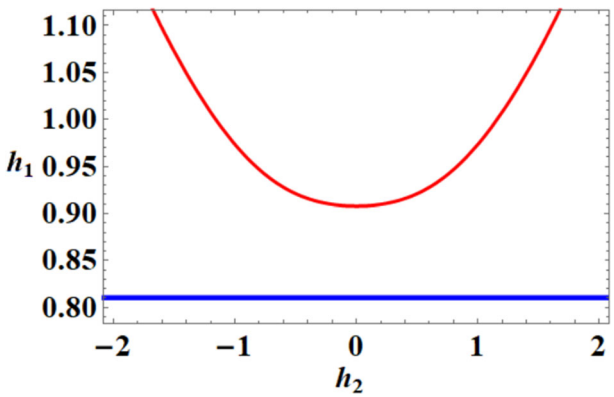

Fig. 13 Displays no fixed points at $\sigma_1 = -0.194$

$$
\begin{aligned}
&- 9\alpha h_{20}^2 + 4(2\sigma_1 + \sigma_2)\omega](C_1 h_{10} + F\ \sin\theta_{10})\cos\theta_{20} + 4\omega[C_1 C_2 \sin\theta_{20} \\
&\times h_{10}^2 + F\ \sin\theta_{10}(2C_1 C_2\omega - (C_1 + C_2)\sin\theta_{20} h_{10}^2)]\} - 8F\omega\cos\theta_{10}[2C_2 \\
&\times \omega l_1 m_1 \sin\theta_{20} h_{10}^2]\},
\end{aligned}
$$

$$
\begin{aligned}
\Gamma_4 = \frac{1}{1024\omega^2}&\{-F h_{10}[(2h_{10}^2 - 9h_{20}^2 + 4(2\sigma_1 + \sigma_2)\omega)\cos\theta_{20} - 4C_2\omega\sin\theta_{20}] \\
&\times [(3h_{10}^2 + 16\sigma_1)\cos\theta_{10} - 8C_1\sin\theta_{10} + 8l_1 m_1\cos\theta_{10}]\}. \qquad (41)
\end{aligned}
$$

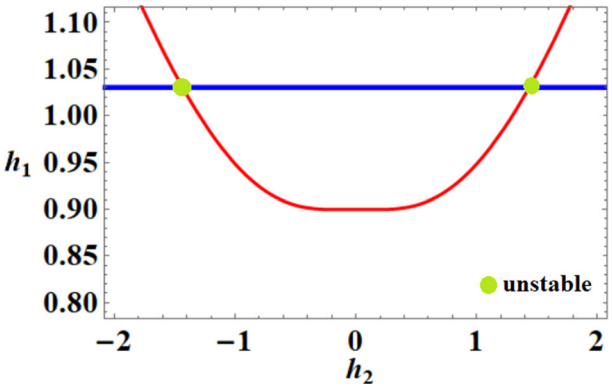

Fig. 14 Reveals two distinct unstable fixed points when $\sigma_1 = -0.17$

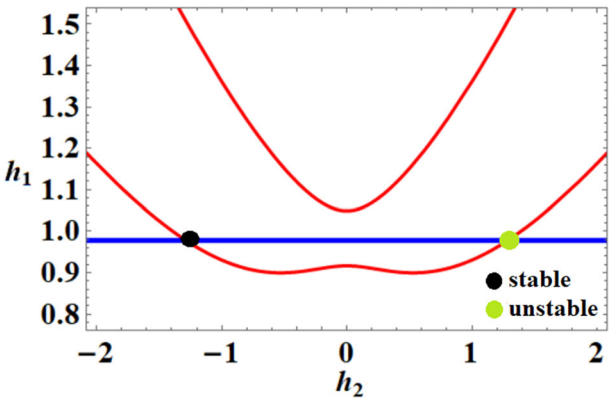

Fig. 15 Explores one possible stable fixed point and one unstable fixed point for the amplitudes h_1 and h_2 at $\sigma_1 = -0.15162$

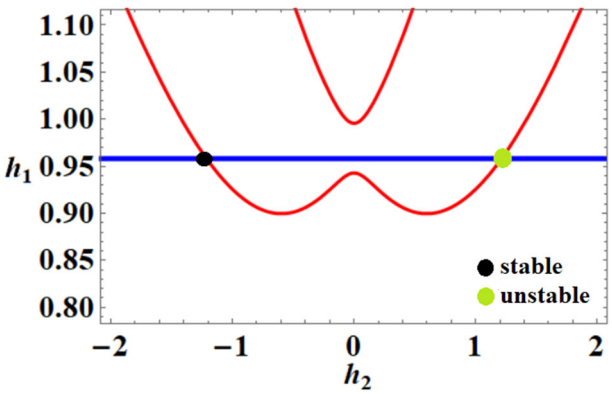

Fig. 16 Explores one possible stable fixed point and one unstable fixed point for the amplitudes h_1 and h_2 at $\sigma_1 = -0.14162$

The criteria of Routh-Hurwitz [10] that outline the necessary and sufficient requirements of the solutions at the steady-state can be stated as follows

$$\begin{aligned} &\Gamma_1 > 0, \qquad \Gamma_3(\Gamma_1\Gamma_2 - \Gamma_3) - \Gamma_1^2\Gamma_4 > 0, \\ &\Gamma_1\Gamma_2 - \Gamma_3 > 0, \qquad \Gamma_4 > 0. \end{aligned} \tag{42}$$

Equations of system (37) have been solved and drawn with different values of σ_1, when $\sigma_2 = -0.0514914$, $C_1 = 0.134975$, and $C_2 = 0.153061$ to yield the curves of Figs. 13, 14, 15, 16 and 17. The blue and red curves represent the first and second equations of system (37), respectively. Intersections of these curves produce fixed points which may be stable or not. The black and green circles express stable and unstable fixed points, respectively. Figures 13, 14, 15, 16, and 17 represent the variation of h_2 versus h_1 when σ_1 has the

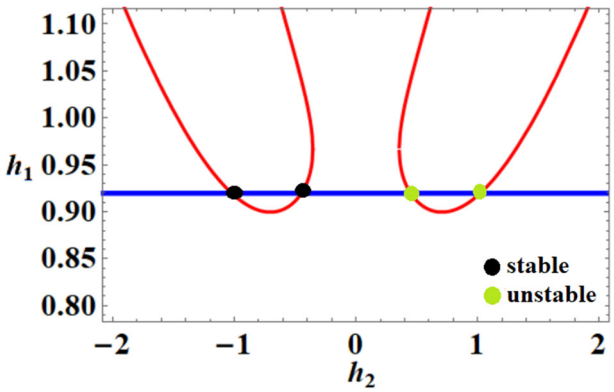

Fig. 17 Shows two possible stable fixed point and two possible unstable fixed points for the amplitudes h_1 and h_2 at $\sigma_1 = -0.13162$

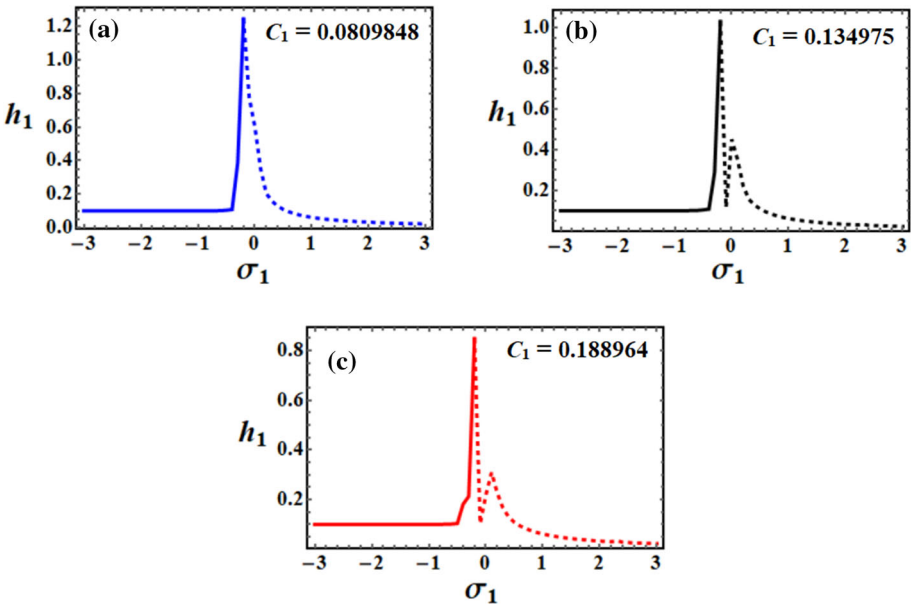

Fig. 18 Shows the resonance curve of $h_1(\sigma_1)$ when $\sigma_2 = 0.192984$: **a** at $C_1 = 0.0809848$, **b** at $C_1 = 0.134975$, **c** at $C_1 = 0.188964$

values -0.194, -0.17, -0.15162, -0.14162, and -0.13162, respectively. Curves of Fig. 13 do not have any fixed points when $\sigma_1 = -0.194$, while the included curves of Fig. 14 have two unstable fixed points at the locations $(-1.458, 1.032)$ and $(1.437, 1.032)$ when $\sigma_1 = -0.17$. Other two fixed points are given in Figs. 15 and 16 at $\sigma_1 = -0.15162$, and $\sigma_1 = -0.14162$, respectively. One of them is stable in each figure at the points $(-1.2961, 0.9791)$ and $(-1.1961, 0.9592)$, while the other is unstable at the locations $(1.284, 0.979)$ and $(1.222, 0.9592)$. On the other hand, the intersections of the curves of Fig. 17 have four fixed points. The stable ones are found at the points $(-0.4493, 0.9193)$ and $(-1.01, 0.9193)$, while the unstable points will be at the locations $(0.447, 0.9193)$ and $(1.026, 0.9193)$.

6 Examination of the stability

The Routh-Hurwitz criteria are used in this part to assess the system's stability and to examine its nonlinear evolution, in which the motion of the model is studied in the presence of the external excitation harmonic moment $M(t)$. Some elements, such as the coefficients of damping C_j $(j = 1, 2)$, the frequencies p, ω, and the parameters of detuning σ_j have been found to have a significant effect on stability operations. A precise procedure involving several system parameters was employed to draw the stability plots of system (34). The modified amplitudes h_j are displayed with σ_j for different parametrical areas when the values $F = 0.140374$,

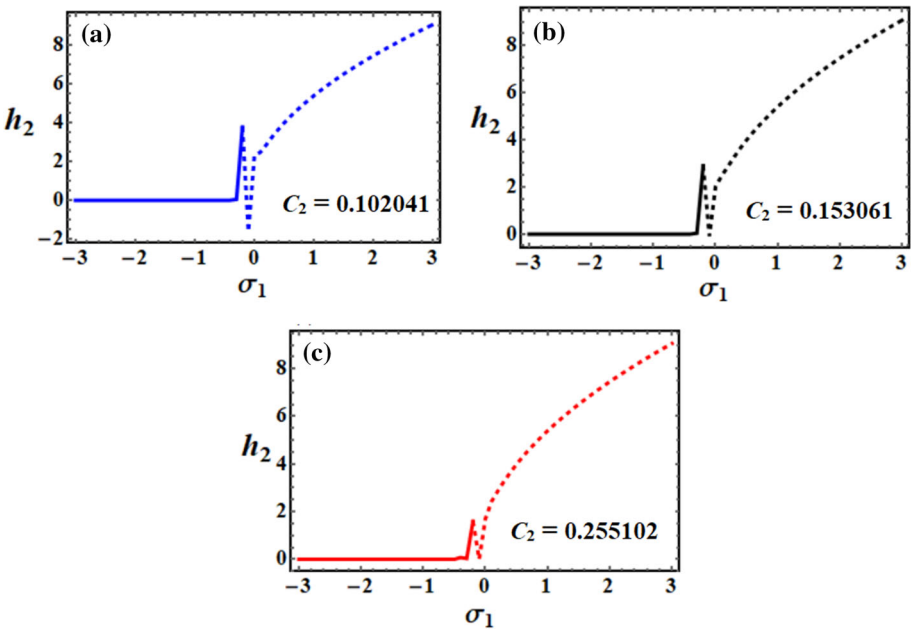

Fig. 19 Demonstrates the frequency response of h_2 as function of σ_1 when $\sigma_2 = 0.192984$: **a** at $C_2 = 0.102041$, **b** at $C_2 = 0.153061$, **c** at $C_2 = 0.255102$

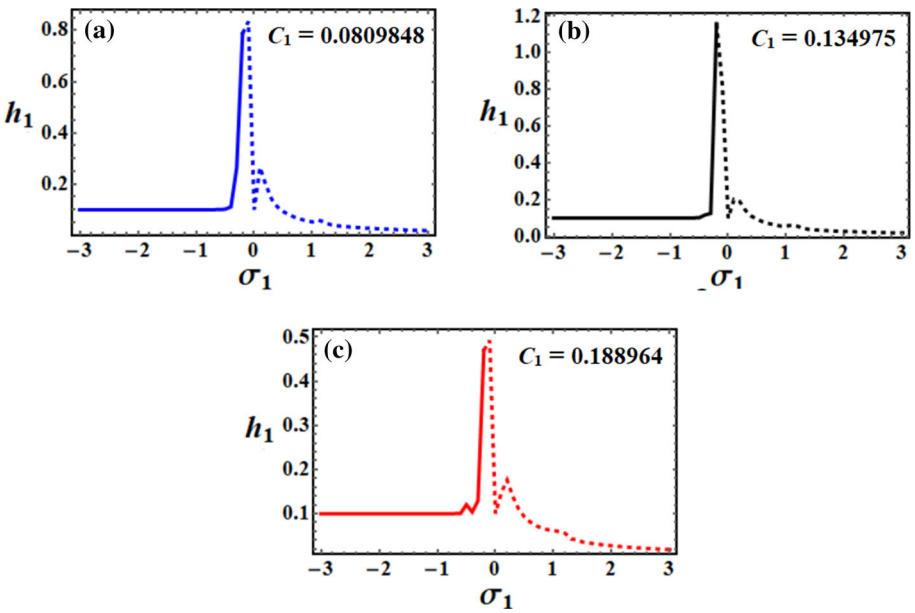

Fig. 20 Sketches $h_1(\sigma_1)$ when $\sigma_2 = 0$: **a** at $C_1 = 0.0809848$, **b** at $C_1 = 0.134975$, **c** at $C_1 = 0.188964$

$C_1(= 0.0809848, 0.134975, 0.188964)$ and $C_2(= 0.102041, 0.153061, 0.255102)$ are considered. Therefore, Figs. 18, 19, 20, 21, 22 and 23 are graphed to characterize the variation of h_j versus σ_1 at distinct values of σ_2 when the coefficients of damping C_j have different values during the specified interval $-3.0 \leq \sigma_1 \leq 3.0$. The influence of variation of C_1 is shown in Figs. 18, 20, and 22 at $\sigma_2 = 0.192984, \sigma_2 = 0$, and $\sigma_2 = -0.05141914$, respectively. Whereas the effect of C_2 is graphed in Figs. 19, 21, and 23 at the same values of σ_2.

The scrutiny of these figures detects that the stability domains of the fixed points are found in the area $-3.0 \leq \sigma_1 \leq -0.2$, while the unstable ones are located in the zone $-0.2 < \sigma_1 \leq 3.0$. The continued curves and the dotted ones are used to represent the stable and unstable points, respectively. The locations of different peaks of fixed points (PFP) and the critical fixed points (CFP) of the response curves of these figures at the

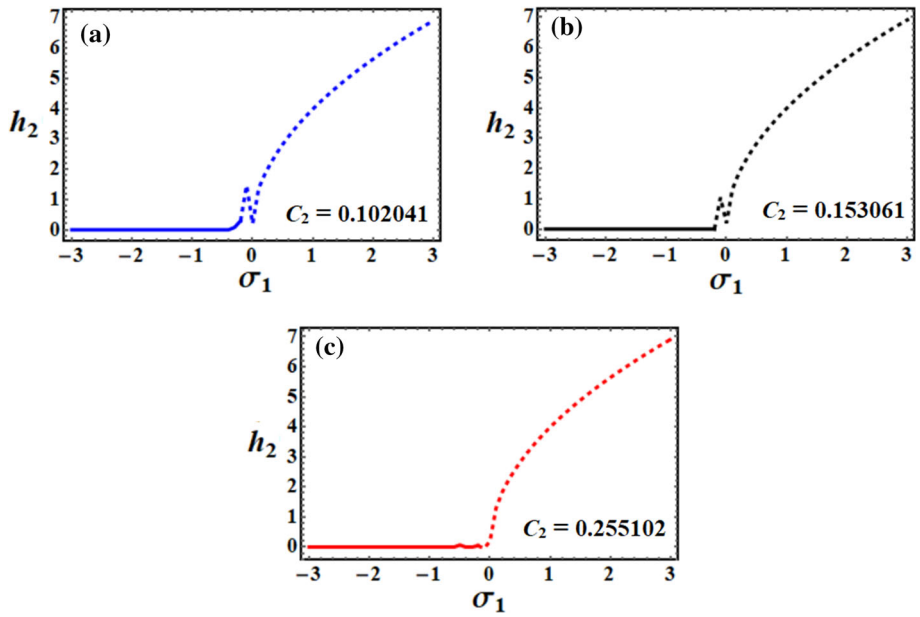

Fig. 21 Explores the resonance curve of h_2 as a function of σ_1 when $\sigma_2 = 0$: **a** at $C_2 = 0.102041$, **b** at $C_2 = 0.153061$, **c** at $C_2 = 0.255102$

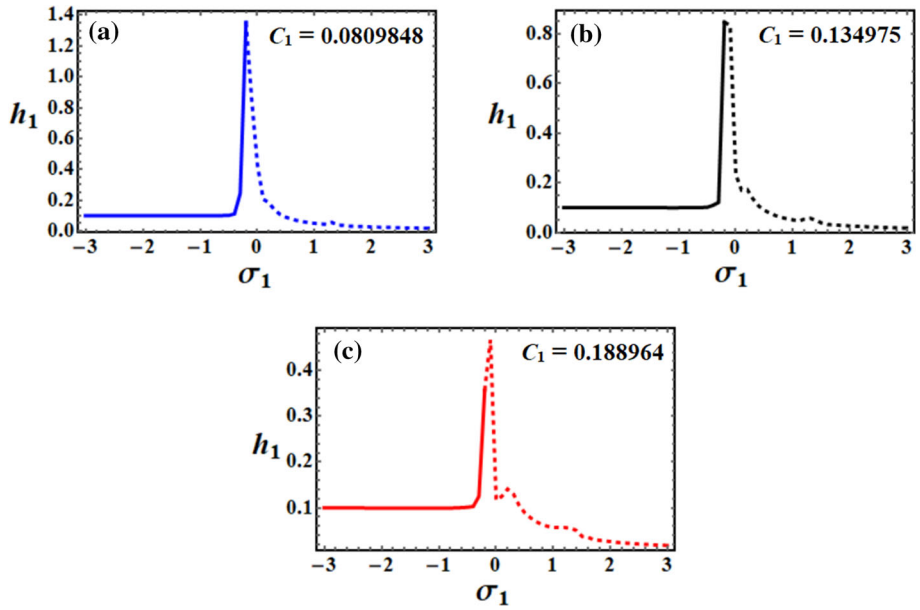

Fig. 22 Displays h_1 via σ_1 when $\sigma_2 = -0.0514914$: **a** at $C_1 = 0.0809848$, **b** at $C_1 = 0.134975$, **c** at $C_1 = 0.188964$

various values of σ_2 are presented in Tables 1, 2, 3, 4, 5 and 6. The CFP is known as that point which is located between the stable and unstable areas, and then it may be stable or not. Moreover, each CFP represent PEP, while the inverse is not necessary.

Figures 24, 25 and 26 describe the resonance curves of h_1 as a function of σ_1, and ther are calculated at $C_1 = 0.0809848$,$C_2 = 0.102041$ when $F(= 0.10798, 0.140374, 0.188964)$, $p_x(= 0.00060609, 0.0303046, 0.0757614)$, $p_y(= 0.0009091, 0.0242437, 0.0606092)$. Moreover, curves of Figs. 24, 25, 26 are drawn when $\sigma_2 = 0.192984$,$\sigma_2 = 0$, and $\sigma_2 = -0.0514914$, respectively. The stability zones of Fig. 24, 25 and 26 are $-3.0 \leq \sigma_1 \leq -0.2$, while the instability areas lie in the domains $-0.2 < \sigma_1 \leq 3.0$. Tables 7, 8 and 9 show the positions of various PFP and CFP for the response curves of Figs. 24, 25 and 26 at various values of $\sigma_2(= 0.192984, 0, -0.0514914)$.

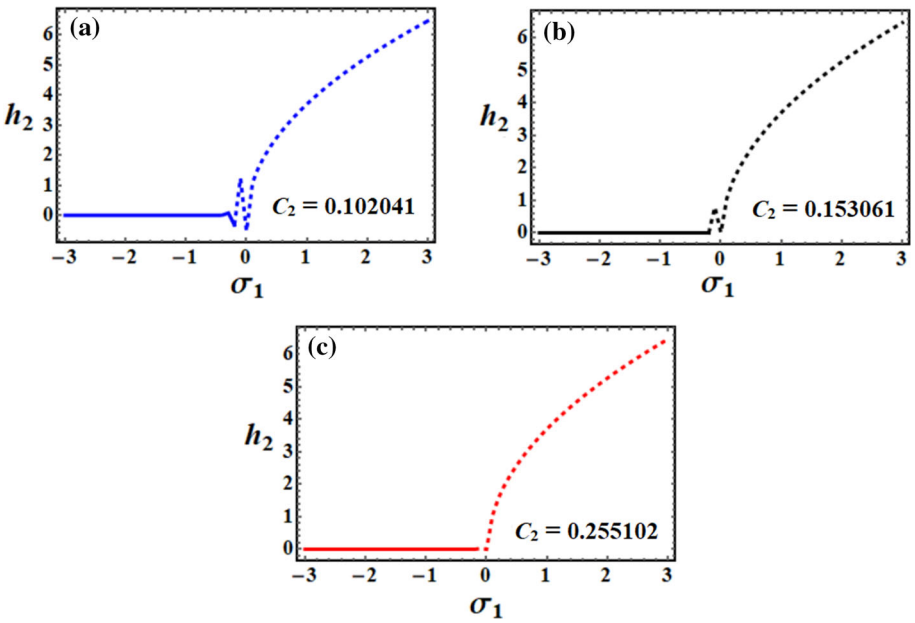

Fig. 23 Describes the variation of the amplitude h_2 versus σ_1 when $\sigma_2 = -0.0514914$: **a** at $C_2 = 0.102041$, **b** at $C_2 = 0.153061$, **c** at $C_2 = 0.255102$

Table 1 Demonstrates the positions of the PFP and the CFP for the response curves at $\sigma_2 = 0.192984$ for the curves of Fig. 18

Figure	PFP	CFP	σ_2
Figure 18a	(− 0..391011, 0.105832) (− 0.184238, 1.25089)	(− 0.184238, 1.25089)	0.192984
Figure 18b	(− 0.403174, 0.110184) (− 0.200626, 1.0473) (− 0.0918118, 0.117015) (0.00340044, 0.452913)	(− 0.200626, 1.0473)	0.192984
Figure 18c	(− 0.500479, 0.0998696) (− 0.384929, 0.179824) (− 0.293706, 0.207501) (− 0.200626, 0.849878) (− 0.10185, 0.113436) (0.0999664, 0.315835)	(− 0.200626, 0.849878)	0.192984

Table 2 Shows the positions of the PFP and the CFP for the response curves of Fig. (19) at $\sigma_2 = 0.192984$

Figure	PFP	CFP	σ_2
Figure 19a	(− 0.308099, 0.07366890) (− 0.186213, 3.85488) (− 0.0914139, − 1.46375) (0.0033857, 2.23436)	(− 0.186213, 3.85488)	0.192984
Figure 19b	(− 0.289412, 0.00585496) (− 0.185354, 3.01606) (− 0.10731, − 0.0283519)	(− 0.185354, 3.01606)	0.192984
Figure 19c	(− 0.397092, 0.074943) (− 0.299787, 0.0272784) (− 0.198361, 1.61391) (− 0.0812955, 0.0547762)	(− 0.198361, 1.61391)	0.192984

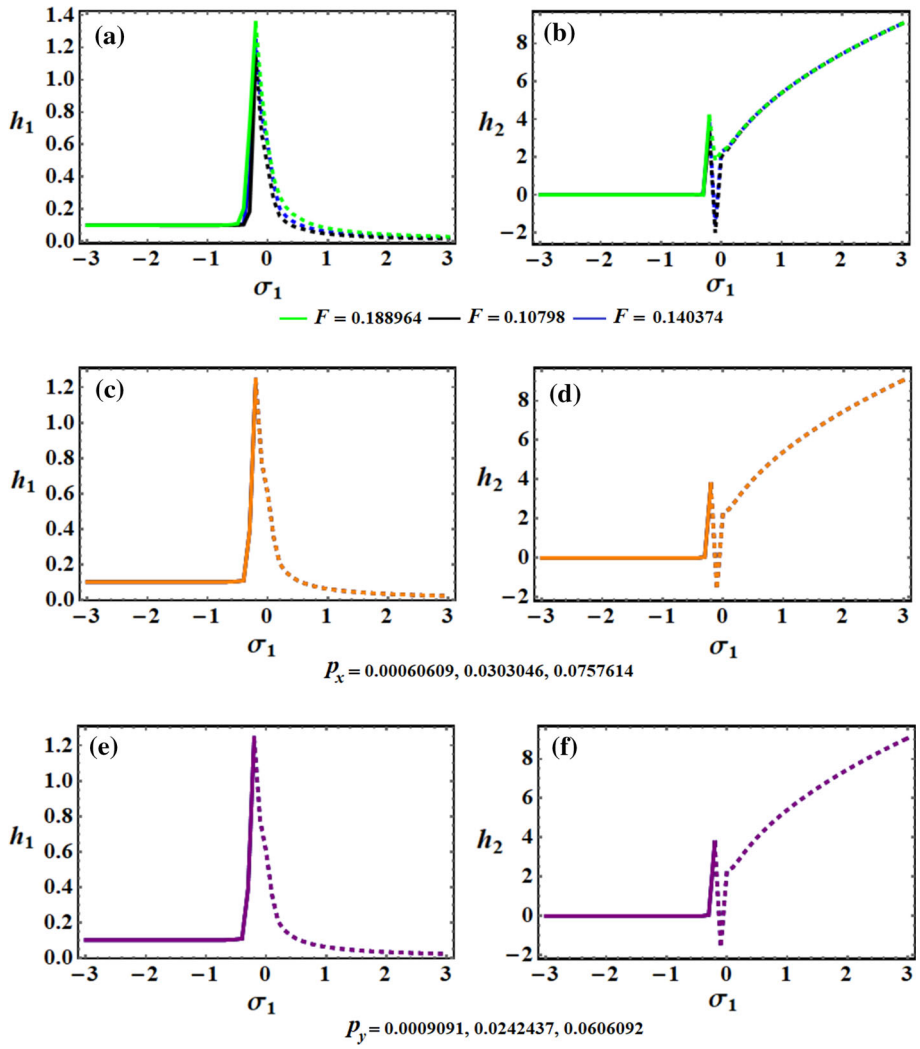

Fig. 24 Describes the resonance curve of $h_j\,(j = 1, 2)$ as a function of σ_1 at $\sigma_2 = 0.192984$: parts **a**, **b** when $F(= 0.10798, 0.140374, 0.188964)$, parts **c**, **d** when $p_x(= 0.00060609, 0.0303046, 0.0757614)$, parts **e** , **f** when $p_y(= 0.0009091, 0.0242437, 0.0606092)$

Table 3 Describes the coordinates of the PFP and the CFP for the response curves of Fig. (20) at $\sigma_2 = 0$.

Figure	PFP	CFP	σ_2
Figure 20a	(− 0.409255, 0.109994) (− 0.196401, 0.790384) (− 0.122032, 0.829729) (0.00340044, 0.101236) (0.112214, 0.258865)	(− 0.196401, 0.790384)	0
Figure 20b	(− 0.299787, 0.123756) (− 0.202482, 1.16459) (− 0.0102013, 0.102463) (0.15302, 0.193026)	(− 0.202482, 1.16459)	0
Figure 20c	(− 0..603865, 0.099717) (− 0..500479, 0.121885) (− 0..397092, 0.103128) (− 0..293706, 0.128706) (− 0..184238, 0.474875) (− 0.108577, 0.489359) (0.0057854, 0.103902) (0.207602, 0.178228)	(− 0.184238, 0.474875)	0

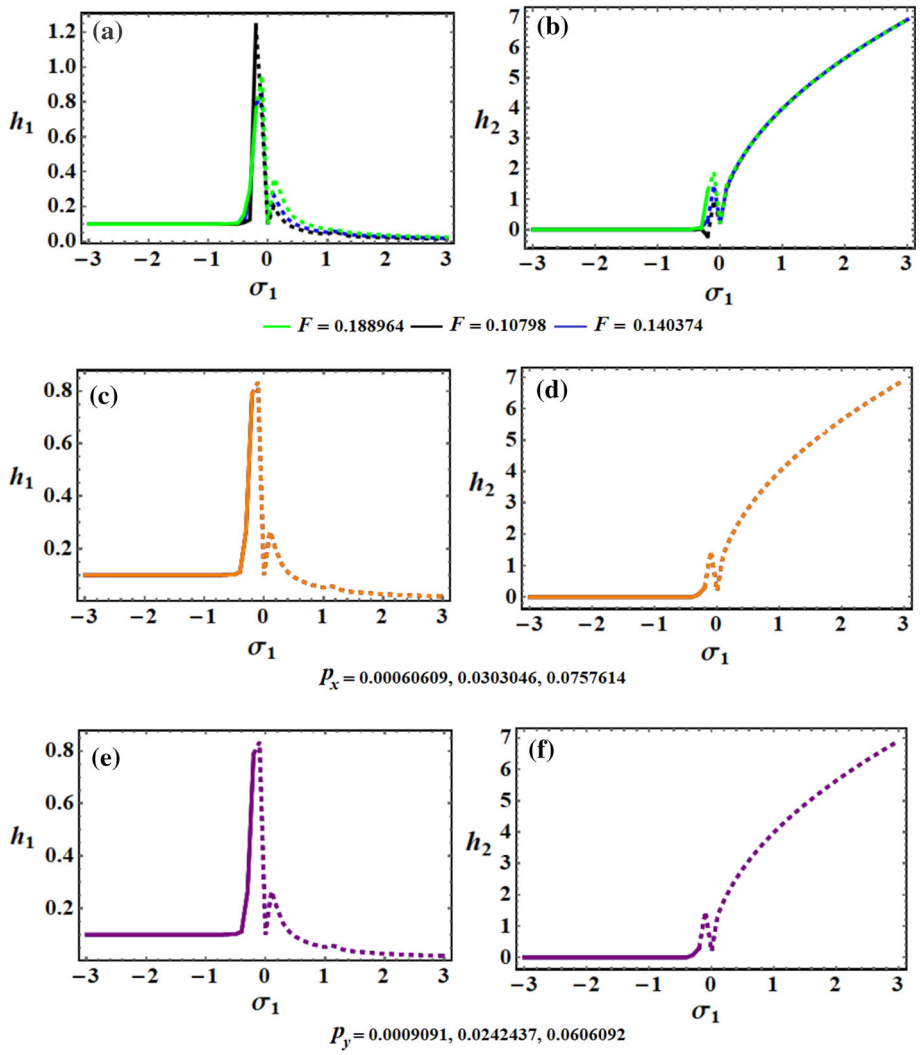

Fig. 25 Explores the resonance curve of h_j $(j = 1, 2)$ as a function of σ_1 at $\sigma_2 = 0$: parts **a** ,**b** for different values of F, parts (c),(d) for different values of p_x, and parts (e),(f) for different values of p_y

Table 4 Explains the positions of the PFP and the CFP for the response curves of Fig. 21 at $\sigma_2 = 0$.

Figure	PFP	CFP	σ_2
Figure 21a	(− 0.224376, 0.282419) (− 0.10731, 1.39554) (0.0227627, 0.230646)	(− 0.224376, 0.282419)	0
Figure 21b	(− 0.198361, -0.00233394) (− 0.10731, 1.05902) (0.00975549, 0.204759)	(− 0.198361, -0.00233394)	0
Figure 21c	(− 0.494397, 0.0714494) (.-0.196401, 0.527472)	(.-0.196401, 0.527472)	0

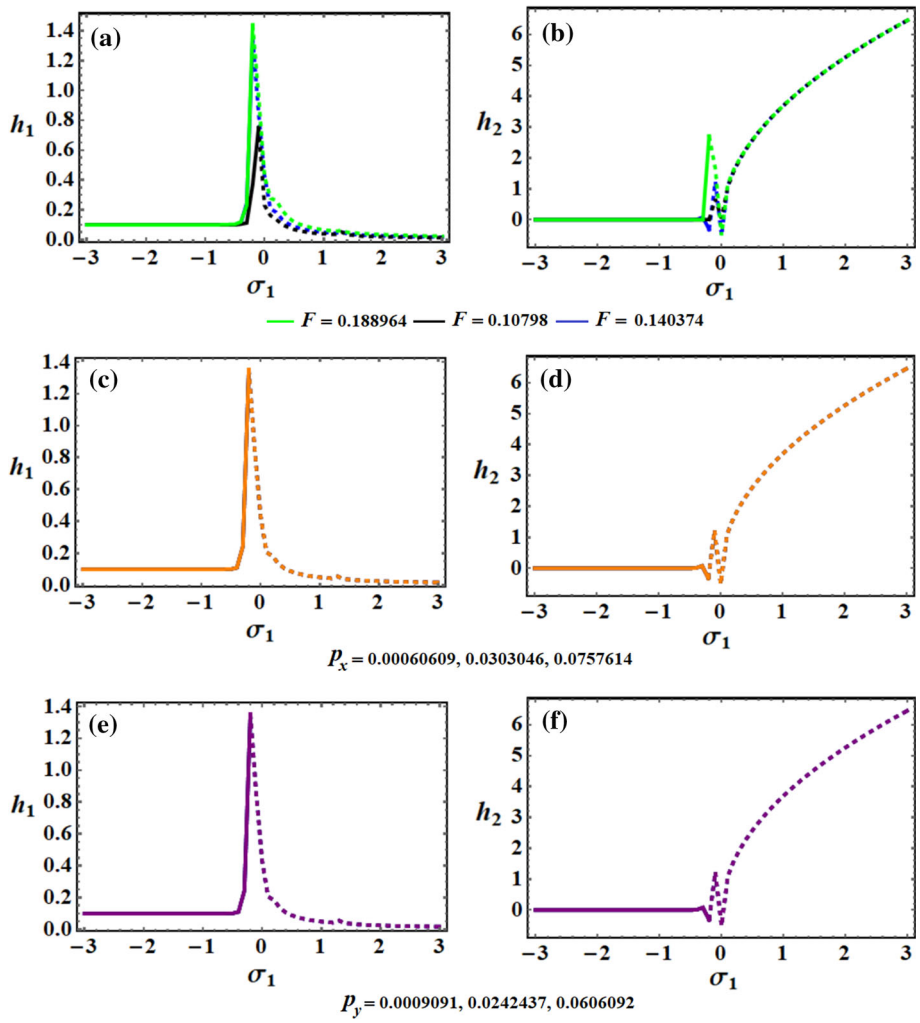

Fig. 26 Shows the resonance curve of h_j $(j = 1, 2)$ as a function of σ_1 at $\sigma_2 = -0.0514914$: parts **a**, **b** for various values of F, parts **c** , **d** for various values of p_x, and parts (**e** , **f** for various values of p_y

Table 5 Displays the coordinates of the PFP and the CFP for the response curves of Fig. 22)at $\sigma_2 = -0.0514914$

Figure	PFP	CFP	σ_2
Figure 22a	(− 0.397092, 0.110284) (− 0.281543, 0.237859) (− 0.190319, 1.3615) (0.0999664, 0.199994)	(− 0.190319, 1.3615)	− 0.0514914
Figure 22b	(− 0.282236, 0.117462) (0.214227, 0.85852) (0.112214, 0.164602)	(0.214227, 0.85852)	− 0.0514914
Figure 22c	(− 0.403174, 0.100322) (− 0.293706, 0.124925) (− 0.10185, 0.461135) (0.0170022, 0.117628) (0.23463, 0.143168)	(− 0.196401, 0.358003)	− 0.0514914

Table 6 Highlights the destinations of the PFP and the CFP for the response curves of Fig. (23) when $\sigma_2 = -0.0514914$

Figure	PFP	CFP	σ_2
Figure 23a	(− 0.299787, 0.0782844) (− 0.196401, − 0.321224) (− 0.09430281, 1.9292) (− 0.003251, -0.528545)	(− 0.196401, − 0.321224)	− 0.0514914
Figure 23b	(− 0.185354, − 0.00930659) (− 0.0812955, 0.71634) (0.00975549, 0.0874464)	(− 0..185354, − 0.00930659)	− 0.0514914
Figure 23c	–	(− 0.0422737, − 0.0334947)	− 0.0514914

Table 7 Shows the locations of the PFP and the CFP for the response curves at $\sigma_2 = 0.192984$ for the curves of Fig. 24

Figure	PFP	CFP	σ_2
Figure 24a	(− 0.404652, 0.103169) (− 0.187024, 1.15527) (− 0.39105, 0.10923) (− 0.200626, 1.25516) (− 0.472661, 0.106736) (− 0.187024, 1.36248)	(− 0.187024, 1.15527) (− 0.200626, 1.25516) (− 0.187024, 1.36248)	0.192984
Figure 24b	(− 0.294556, 0.037748) (− 0.186213, 3.4868) (− 0.0914139, − 1.98857) (0.0304713, 2.10718) (− 0.321641, − 0.00943457) (− 0.199756, 3.8133) (− 0.104957, − 1.5053) (0.0169285, 2.1097) (− 0.276405, − 0.0130093) (− 0.198361, 4.2916) (− 0.0812955, 1.88509)	(− 0.186213, 3.4868) (− 0.199756, 3.81333) (− 0.198361, 4.2916)	0.192984
Figure 24c	(− 0.39105, 0.10923) (− 0.200626, 125516) (− 0.350245, 0.109231) (− 0.200626, 1.25054) (− 0.363847, 0.0999894) (− 0.187024, 1.25054)	(− 0.200626, 1.25516) (− 0.200626, 1.25554)	0.192984
Figure 24d	(− 0.321641, − 0.00943457) (− 0.199756, 3.8133) (− 0.104957, − 1.5053) (0.0169285, 2.1097) (− 0.281013, − 0.0509863) (− 0.186213, 3.81333) (− 0.0914139, − 1.54685) (0.0101351, 2.2504) (− 0.281013, 0.0321172) (− 0.186213, 3.85488) (− 0.0914139, − 1.46375) (0.0033857, 2.23436)	(− 0.199756, 3.81333) (− 0.186213, 3.81333) (− 0. 186213, 3.85488)	0.192984
Figure 24e	(− 0.39105, 0.10923) (− 0.200626, 125516) (− 0.380849, 0.105765) (− 0.197225, 1.25632) (− 0.38552, 0.105379) (− 0.192776, 1.2497)	(− 0.200626, 1.25516) (− 0.197225, 1.25632) (− 0.192776, 1.2497)	0.192984

Table 7 continued

Figure	PFP	CFP	σ_2
Figure 24f	(− 0.321641, − 0.00943457) (− 0.199756, 3.8133) (− 0.104957, − 1.5053) (0.0169285, 2.1097) (− 0.278566, − 0.144181) (− 0.197528, 3.83945) (− 0.106361, − 1.53732) (0.00506483, 2.22331) (− 0.268436, 0.016615) (− 0.197528, 3.87053) (0.0962318, − 1.50624) (0.0151945, 2.22331)	(− 0.199756, 3.81333) (− 0.197528, 3.83945) (− 0.197528, 3.87053)	0.192984

Table 8 Presents the locations of the PFP and the CFP for the response curves at $\sigma_2 = 0$ for the curves of Fig. 25

Figure	PFP	CFP	σ_2
Figure 25a	(− 0.268634, 0.120127) (− 0.200626, 1.25403) (0.00340044, 0.101539) (0.112214, 0.21307) (− 0.404652, 0.110509) (− 0.0918118, 0.833747) (0.00340044, 0.101236) (0.112214, 0.258865) (− 0.486262, 0.103274) (− 0.105413, 0.94891) (0.00340044, 0.0997502) (0.0986126, 0.367535)	(− 0.200626, 1.25403) (− 0.200626, 0.790477) (− 0.187024, 0.772735)	0
Figure 25b	(− 0.302419, 0.0672743) (− 0.198361, 0.300746) (− 0.0812955, 0.868745) (0.00975546, 0.200853) (− 0.0943028, 1.42143) (0.022767, 0.256532) (− 0.289412, − 0.00240918) (− 0.0812955, 1.86145) (0.0097546, 0.204686)	(− 0.198361, − 0.300746) (− 0.185354, 0.385965) (− 0.172347, 1.3696)	0
Figure 25c	(− 0.404652, 0.110509) (− 0.0918118, 0.833747) (0.00340044, 0.101236) (0.112214, 0.258865) (− 0.377448, 0.1074108) (− 0.105413, 0.836838) (0.00340044, 0.0981456) (0.0986126, 0.0252684) (− 0.363847, 0.113599) (− 0.0918117, 0.833747) (0.0170022, 0.104377) (0.112214, 0.255775)	(− 0.200626, 0.790477) (− 0.200626, 0.78495) (− 0.187024, 0.793567)	0
Figure 25d	(− 0.0943028, 1.42143) (0.022767, 0.256532) (− 0.0943028, 1.39554) (0.0227627, 0.256532) (− 0.10731, 0.142143) (0.00650365, 0.237117)	(− 0.185354, 0.385965) (− 0.1853541, 0.360079) (− 0.185354, 0.308306)	0

Table 8 continued

Figure	PFP	CFP	σ_2
Figure 25e	(− 0.404652, 0.110509) (− 0.0918118, 0.833747) (0.00340044, 0.101236) (0.112214, 0.258865) (− 0.385552, 0.108517) (− 0.101461, 0.837064) (0.0101461, 0.1016) (0.11607, 0.260682) (− 0.36526, 0.108517) (− 0.111607, 0.837064) (0.0101461, 0.09922946) (0.131899, 0.258376)	(− 0.200626, 0.790477) (− 0.192776, 0.788648)	0
Figure 25f	(− 0.0943028, 1.42143) (0.022767, 0.256532) (− 0.0923406, 1.41911) (0.0243002, 0.219746) (− 0.102061, 1.39976) (0.0145801, 0.200401)	(− 0.185354, 0.385965) (− 0.189541, 0.316468) (− 0.199261, 0.316468)	0

Table 9 Gives the positions of the PFP and the CFP for the response curves at $\sigma_2 = -0.0514914$ for the curves of Fig. 26

Figure	PFP	CFP	σ_2
Figure 26a	(− 0.295838, 0.1078713) (− 0.105413, 0.755748) (1.29557, 0.0492287) (− 0.39105, 0.108455) (− 0.187024, 1.36209) (− 0.369843, 0.121979) (− 0.179832, 1.44755) (− 0.132329, 0.27164)	(− 0.105413, 0.755748) (− 0.202922, 1.36418) (− 0.179832, 1.44755)	− 0.0514914
Figure 26b	(− 0.88361, 0.0390682) (− 0.0943028, 0.692148) (0.0227627, 0.111633) (− 0.296462, 0.136059) (− 0.189541, − 0.39118) (− 0.0923406, 1.22946) (0.00486003, − 0.488743) (− 0.289412, 0.02978291) (− 0.198361, 2.76917) (0.00975546, -0.518095)	(− 0.198361, 0.0390682) (− 0.189541, -0.39118) (− 0.198361, 2.76917)	− 0.0514914
Figure 26c	(− 0.39105, 0.108455) (− 0.187024, 1.36209) (− 0.385552, 0.104751) (− 0.92776, 1.36418)	(− 0.202922, 1.36418) (− 0.192776, 1.36418)	− 0.0514914
Figure 26d	(− 0.296462, 0.136059) (− 0.189541, − 0.39118) (− 0.0923406, 1.22946) (0.00486003, − 0.488743) (− 0.296462, 0.136059) (0.189541, − 0.410643) (− 0.09234061, 1.22946) (0.00486003, − 0.488743)	(− 0.189541, − 0.39118)	− 0.0514914
Figure 26e	(− 0.39105, 0.108455) (− 0.187024, 1.36209) (− 0.395698, 0.104751) (− 0.202922, 1.36795) (− 0.385552, 0.108521) (− 0.213068, 1.36041)	(− 0.202922, 1.36418) (− 0.202922, 1.36795) (− 0.213068, 1.36041)	− 0.0514914

Table 9 continued

Figure	PFP	CFP	σ_2
Figure 26f	(− 0.296462, 0.136059) (− 0.189541, − 0.39118) (− 0.0923406, 1.22946) (0.00486003, − 0.488743) (− 0.296462, 0.116534) (− 0.17982, 0.371592) (− 0.0923406, 1.22946) (0.00486003, − 0.488743) (− 0.296462, 0.116536) (− 0.199261, − 0.371592) (− 0.102061, 1.24899) (0.00486003, − 0.449693)	(− 0.189541, − 0.39118) (− 0.17982, − 0.371592) (− 0.199261, − 0.371592)	− 0.0514914

7 Conclusion

The planar motion of a 2DOF dynamical system consisting of a coupled tuned longitudinal absorber with a simple pendulum in the presence of a harmonic excitation moment has been examined. The pendulum's pivot has been forced to follow a Lissajous trajectory with constant angular velocity. The governing system of the EOM has been derived applying the equations of Lagrange of the second kind. One of the most accurate perturbation approaches, called AMS has been used to achieve the solutions of this system up to a greater order of approximation. The different types of resonance cases have been categorized, and two of them have been studied at the same time. The equations of modulation have been obtained in view of the system's solvability criteria. These equations have been reduced to an algebraic system of two nonlinear algebraic equations which are solved numerically and graphed to obtain all possible fixed points. The stability of these points at the steady-state has been examined based on the criteria of Routh-Hurwitz. The solutions' temporal histories, altered phases and amplitudes, and resonance curves have been drawn to analyze the dynamical manner at any moment. The effect of the various parameters on the system's behavior has been assessed through the examination of the various stability areas. The calculations have been performed using the computer's codes and Wolfram Mathematica software. The gained results can be considered novel, in which the used methodology has been applied to a specific dynamical system. The weight of the examined dynamical system can be seen from its numerous applications in real life, particularly in the reduction in vibrations in diverse engineering constructions.

Acknowledgements There was no explicit support for this study from any government, commercial, or non-profit organization.

Authors contribution TSA: Supervision, Resources, Conceptualization, Methodology, Validation, Data curation, Visualization and Reviewing. SAA: Supervision, Conceptualization, Resources, Formal analysis, Visualization and Reviewing. RFE: Investigation, Formal analysis, Visualization, Writing- Original draft preparation.

Funding Open access funding provided by The Science, Technology & Innovation Funding Authority (STDF) in cooperation with The Egyptian Knowledge Bank (EKB).

Data Availability The datasets used and/or analyzed during the current study available from the corresponding author on reasonable request.

Declaration

Conflict of interest The authors have indicated that they have no conflicts of interest.

References

1. Meirovitch, L.: Fundamental of Vibrations. McGraw-Hill, New York (2001)
2. Tondl, A., Nabergoj, R.: Dynamic absorbers for an externally excited pendulum. J. Sound Vib. **234**, 611–624 (2000)
3. Arfiadi, Y., Hardi, N.S.: Passive and active control of three-dimensional buildings. Earthq. Eng. Struct. Dyn. **29**, 388–396 (2000)
4. Nagashima, I.: Optimal displacement feedback control law for active tuned mass damper. Earthq. Eng. Struct. Dyn. **30**(8), 1221–1242 (2001)
5. Eissa, M., Sayed, M.: A comparison between active and passive vibration control of non-linear simple pendulum, part I: transversally tuned absorber and negative feedback. Math. Comput. Appl. **11**(2), 137–149 (2006)
6. Eissa, M., Sayed, M.: A comparison between active and passive vibration control of non-linear simple pendulum, part II: longitudinal tuned absorber and negative and feedback. Math. Comput. Appl. **11**(2), 151–162 (2006)
7. Amer, W.S., Bek, M.A., Abohamer, M.K.: On the motion of a pendulum attached with tuned absorber near resonances. Results Phys. **11**, 291–301 (2018)
8. Amer, W.S., Amer, T.S., Hassan, S.S.: Modeling and stability analysis for the vibrating motion of three degrees-of-freedom dynamical system near resonance. Appl. Sci. **11**(24), 11943 (2021)
9. Eissa, M., Sayed, M.: Vibration reduction of a three DOF non-linear spring pendulum. Commun. Nonlinear Sci. Numer. Simul. **13**(2), 465–488 (2008)
10. Strogatz, S.H.: Nonlinear Dynamics and Chaos: With Applications to Physics, Biology, Chemistry, and Engineering, 2nd edn. Princeton University Press, Princeton (2015)
11. Wang, L., Shi, W., Zhou, Y.: Study on self-adjustable variable pendulum tuned mass damper. Struct. Des. Tall Spec. Build. **28**(1), e1561 (2019)
12. Wang, L., Nagarajaiah, S., Shi, W., Zhou, Y.: Study on adaptive-passive eddy current pendulum tuned mass damper for wind-induced vibration control. Struct. Des. Tall Spec. Build. **29**(15), e1793 (2020)
13. Wang, L., Shi, W., Li, X., Zhang, Q., Zhou, Y.: An adaptive-passive retuning device for a pendulum tuned mass damper considering mass uncertainty and optimum frequency. Struct. Contr. Health. Monit. **26**(7), e2377 (2019)
14. Wang, L., Shi, W., Zhou, Y., Zhang, Q.: Semi-active eddy current pendulum tuned mass damper with variable frequency and damping. Smart Struct. Syst. **25**(1), 65–80 (2020)
15. Wang, L., Shi, W., Zhou, Y.: Adaptive-passive tuned mass damper for structural aseismic protection including soil-structure interaction. Soil Dyn. Earthq. Eng. **158**, 107298 (2022)
16. Shi, W., Wang, L., Lu, Z.: Study on self-adjustable tuned mass damper with variable mass. Struct. Control Health Monit. **25**(3), e2114 (2018)
17. Shi, W., Wang, L., Lu, Z., Wang, H.: Experimental and numerical study on adaptive-passive variable mass tuned mass damper. J. Sound Vib. **452**, 97–111 (2019)
18. Wang, L., Nagarajaiah, S., Shi, W., Zhou, Y.: Semi-active control of walking-induced vibrations in bridges using adaptive tuned mass damper considering human-structure-interaction. Eng. Struct. **244**, 112743 (2021)
19. Gitterman, M.: Spring pendulum: Parametric excitation vs an external force. Physica A **389**, 3101–3108 (2010)
20. Belyakov, A.O.: On rotational solutions for elliptically excited pendulum. Phys. Lett. A **375**, 2524–2530 (2011)
21. Amer T. S., Bek M. A., Hamada I. S.: On the motion of harmonically excited spring pendulum in elliptic path near resonances, Adv. Math. Phys., vol. 2016, (2016), Article ID 8734360, 15 pages.
22. Starosta, R., Kamińska, G.S., Awrejcewicz, J.: Asymptotic analysis of kinematically excited dynamical systems near resonances. Nonlinear Dyn. **68**, 459–469 (2012)
23. Awrejcewicz, J., Starosta, R., Kaminska, G.: Asymptotic analysis of resonances in nonlinear vibrations of the 3-dof pendulum. Differ. Equ. Dyn. Syst. **21**, 123–140 (2013)
24. Amer, T.S., Bek, M.A., Abouhmr, M.K.: On the vibrational analysis for the motion of a harmonically damped rigid body pendulum. Nonlinear Dyn. **91**, 2485–2502 (2018)
25. Amer, T.S., Bek, M.A., Abouhmr, M.K.: On the motion of a harmonically excited damped spring pendulum in an elliptic path. Mech. Res. Commu. **95**, 23–34 (2019)
26. El-Sabaa, F.M., Amer, T.S., Gad, H.M., Bek, M.A.: On the motion of a damped rigid body near resonances under the influence of harmonically external force and moments. Results Phys. **19**, 103352 (2020)
27. Abady, I.M., Amer, T.S., Gad, H.M., Bek, M.A.: The asymptotic analysis and stability of 3DOF non-linear damped rigid body pendulum near resonance. Ain Shams Eng. J. **13**(2), 101554 (2022)
28. Amer, W.S.: The dynamical motion of a rolling cylinder and its stability analysis: analytical and numerical investigation. Arch. Appl. Mech. (2022). https://doi.org/10.1007/s00419-022-02236-9
29. Amer, W.S.: Modelling and analyzing the rotatory motion of a symmetric gyrostat subjected to a Newtonian and magnetic fields. Results Phys. **24**, 104102 (2021)
30. Ismail A. I.: Treating the solid pendulum motion by the large parameter procedure. Int. J. Aerosp. Eng. vol. (2020), Article ID 8853867, 8 pages
31. Amer T. S.: The dynamical behavior of a rigid body relative equilibrium position, Adv. Math. Phys., vol. (2017), Article ID 8070525, 13 Pages
32. Ismail, A.I.: A new pendulum motion with a suspended point near infinity. Sci. Rep. **11**, 13199 (2021)
33. Amer, T.S., Starosta, R., Elameer, A.S., Bek, M.A.: Analyzing the stability for the motion of an unstretched double pendulum near resonance. Appl. Sci. **11**, 9520 (2021)
34. Amer, T.S., Starosta, R., Almahalawy, A., Elameer, A.S.: The stability analysis of a vibrating auto-parametric dynamical system near resonance. Appl. Sci. **12**, 1737 (2022)

35. Amer, T.S., Bek, M.A., Hassan, S.S.: Elbendary sherif the stability analysis for the motion of a nonlinear damped vibrating dynamical system with three-degrees-of-freedom. Results Phys. **28**, 104561 (2021)
36. Ji-Huan, He., Amer, T.S., Abolila, A.F., Galal, A.A.: Stability of three degrees-of-freedom auto-parametric system. Alex. Eng. J. **61**(11), 8393 (2022)
37. Abdelhfeez, S.A., Amer, T.S., Elbaz, R.F., Bek, M.A.: Studying the influence of external torques on the dynamical motion and the stability of a 3DOF dynamic system. Alex. Eng. J. **61**(9), 6695–6724 (2022)
38. Bek, M.A., Amer, T.S., Sirwah Magdy, A., Awrejcewicz, J., Arab, A.A.: The vibrational motion of a spring pendulum in a fluid flow. Results Phys. **19**, 103465 (2020)
39. Nayfeh, A.H.: Perturbation Methods. Wiley-VCH Verlag GmbH and Co. KgaA, Weinheim (2008)
40. He, C.-H., Amer, T.S., Tian, D., Abolila, A.F., Galal, A.A.: Controlling the kinematics of a spring-pendulum system using an energy harvesting device. J. Low Freq. Noise V. A. (2022). https://doi.org/10.1177/14613484221077474
41. Amer, W.S., Amer, T.S., Starosta, R., Bek, M.A.: Resonance in the cart-pendulum system-an asymptotic approach. Appl. Sci. **11**(23), 11567 (2021)